Geological Society of America Bulletin, published online on 27 April 2016 as doi:10.1130/B31419.1

THE GEOLOGICAL SOCIETY OF AMERICA®

Rapid exhumation of the eastern Himalayan syntaxis since the late Miocene

Karl A. Lang[1,†], Katharine W. Huntington[1], Russ Burmester[2], and Bernard Housen[2]

[1]*Department of Earth and Space Sciences and Quaternary Research Center, University of Washington, 4000 15th Avenue NE, Johnson Hall Room 070, Box 351310, Seattle, Washington 98195-1310, USA*

[2]*Department of Geology, Western Washington University, 516 High Street, Environmental Studies Room 240, Bellingham, Washington 98225-9080, USA*

ABSTRACT

The Himalayan syntaxes are exceptionally dynamic landscapes characterized by high-relief topography and some of the most rapid and focused crustal exhumation on Earth. In the eastern Himalayan syntaxis, it has been hypothesized that thermomechanical feedbacks between erosion by the Yarlung River and growth of a crustal-scale antiform may have locally sustained exhumation rates exceeding 5 km/m.y. during the late Pliocene and Pleistocene. However, young (younger than 3 Ma) cooling histories from syntaxial bedrock samples restrict interpretations of the timing and mechanism initiating feedback development. To extend this record of landscape evolution, we reconstructed an exhumation history since the late Miocene from analysis of detrital minerals in Himalayan foreland basin deposits. We combined magnetostratigraphy, detrital white mica $^{40}Ar/^{39}Ar$ thermochronology, and coupled zircon U-Pb and fission-track geothermochronology from a 4.6-km-thick stratigraphic section proximal to the eastern syntaxis. We used a simple thermal model to interpret the combined provenance and lag-time data set, concluding that rock exhumation rates in the core of the syntaxis increased by a factor of 5–10 in the late Miocene and have sustained extremely rapid exhumation rates (>5 km/m.y.) since 5 Ma. This onset significantly postdates the first appearance of Tibetan detritus in the Himalayan foreland, suggesting that thermomechanical feedbacks sustaining rapid exhumation are unrelated to river integration. Instead, such feedbacks may develop where large, antecedent rivers sustain elevated erosion rates across a region of enhanced rock uplift. Compilation of similar data sets across the Himalaya demonstrates extraordinary syntaxial exhumation histories, potentially resulting from peculiar geodynamics at these orogenic margins.

INTRODUCTION

The evolution of mountain landscapes reflects complex relationships between tectonic processes transferring mass within Earth's interior and erosional processes redistributing mass across Earth's surface (e.g., Davis et al., 1983; Koons, 1990; Beaumont et al., 1992). Numerical (e.g., Willet, 1999; Beaumont et al., 2000), analog (e.g., Mugnier et al., 1997; Marques and Cobbold, 2002; Hoth et al., 2006), and analytical (e.g., Whipple and Meade, 2004; Simpson, 2006) experiments document the dynamic influence of erosion and deposition on crustal deformation from local to orogenic scales. Erosion may influence crustal deformation patterns by locally reducing lithospheric stress (Simpson, 2004) to locally promote crustal-scale folding (Burg and Podladchikov, 2000) and thrust faulting (Burg and Schmalholz, 2008). The resulting rock uplift steepens topographic features, including river channels (Whipple and Tucker, 1999), elevating erosion rates to exhume crustal material (Ring et al., 1999). When rapid crustal exhumation remains focused for a prolonged period, elevation of the geothermal gradient (Koons et al., 2002) may be sufficient to initiate a thermo-mechanical feedback that sustains steep topography perched above hot, actively deforming crust (Zeitler et al., 2001; Koons et al., 2013).

A concomitance of steep topography (Burbank et al., 1996; Larsen and Montgomery, 2012), elevated geothermal gradients (Winslow et al., 1994; Craw et al., 2005), and active crustal-scale structures (Burg et al., 1998; Schneider et al., 1999a) is locally observed at both ends of the Himalayan orogen. In these regions, margin-normal motion of the Indian-Eurasian plate collision transitions to strike-slip motion, warping terranes southward to form broad syntaxes (Fig. 1A; Wadia, 1931; Gansser, 1966; Treloar and Coward, 1991). Rivers flowing parallel to the orogen in southern Tibet cross the Himalaya through these syntaxes, dramatically steepening (Finlayson et al., 2002) as they bisect young metamorphic massifs (Zeitler et al., 1982; Burg et al., 1998). Bedrock thermochronology from both regions indicates rapid cooling of these massifs during the late Pliocene and Pleistocene (e.g., Zeitler et al., 1993; Winslow et al., 1996; Burg et al., 1998; Malloy, 2004; Zeitler et al., 2014), and bedrock geochronology further suggests that localized anatexis related to massif decompression has been ongoing since the late Miocene (e.g., Schneider et al., 1999b; Booth et al., 2004). However, detailed exhumation histories of these regions are difficult to interpret from rapidly exhumed bedrock samples alone. Instead, detrital cooling ages from proximal foreland basin units are useful for documenting earlier Neogene exhumation and have been successfully applied in the western syntaxis (e.g., Cerveny et al., 1988; Najman et al., 2003; also see Bernet and Garver, 2005; Ruiz and Seward, 2006), yet comparable analyses from the eastern Himalaya are lacking.

Some detrital cooling ages are available from eastern Himalayan foreland basin units (Chirouze et al., 2012a, 2013); however, the distal

†Present address: Department of Geosciences, University of Tübingen, Wilhelmstraße 56, Lothar Meyer Bau Room 250, Tübingen 72076, Germany; karl.lang@ifg.uni-tuebingen.de.

GSA Bulletin; doi: 10.1130/B31419.1; 12 figures; Data Repository item 2016103.

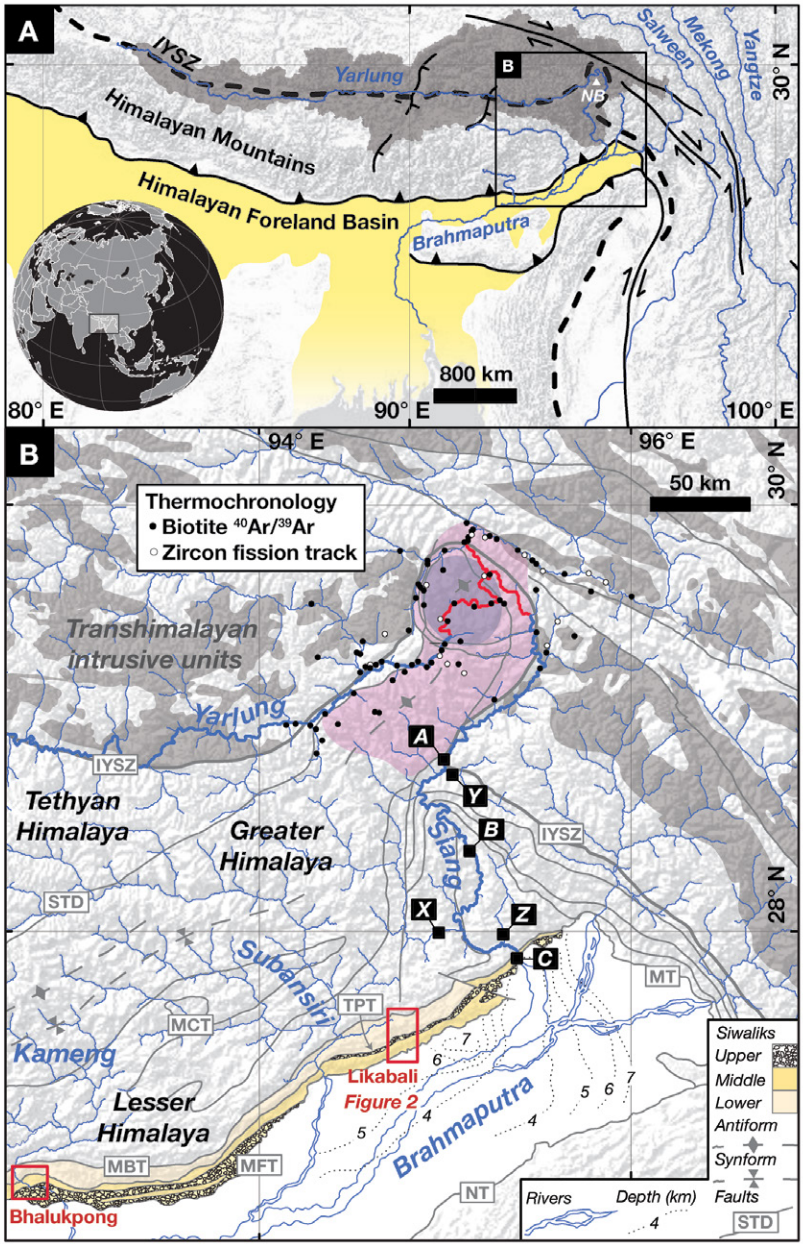

Figure 1. (A) Map of the study area showing the Indus-Yarlung suture zone (IYSZ; dashed line) and rivers surrounding the eastern Himalayan syntaxis. The Yarlung River turns southward around the Namche Barwa massif (NB, 7782 m peak elevation), to join the Brahmaputra River in the Himalayan foreland basin (yellow area). (B) The Tsangpo Gorge (red line) bisects the Namche Barwa massif (purple area from Zeitler et al., 2014), a source of anomalously young cooling ages (pink area encompasses zircon fission-track ages younger than 3 Ma and biotite $^{40}Ar/^{39}Ar$ ages younger than 10 Ma (see text for data references). Black squares indicate sample locations for modern detrital white mica from the Siang River (A, B, C) and Himalayan tributaries (X, Y, Z). Red boxes outline sections studied by us (see Figs. 2 and 3) and by Chirouze et al. (2012a). Basin depth contours are from Verma and Mukhopadhyay (1977). Structure abbreviations: MCT—Main Central thrust; MFT—Main Frontal thrust; MBT—Main Boundary thrust; STD—South Tibetan detachment; TPT—Tipi thrust; NT—Naga thrust; MT—Mishmi thrust. Contacts are compiled from Armijo et al. (1989); Agarwal et al. (1991); Baruah et al. (1992); Pan et al. (2004); Acharyya (2007); Misra (2009); Yin et al. (2010); and Zeitler et al. (2014).

position of these samples complicates an otherwise straightforward interpretation of their provenance. Chirouze et al. (2013) collected samples from exposures along the Kameng River, an eastern Himalayan tributary to the Brahmaputra ~300 km downstream from its range-front confluence. In this section, Nd and Hf isotope measurements indicate a sedimentary provenance similar to the modern Brahmaputra River between 7 and 3 Ma. At this stratigraphic interval, Chirouze et al. interpreted 1.9–4.0 m.y. thermochronologic lag times to reflect source-region exhumation rates ranging between ~1 and 4 km/m.y. These data may indicate that the young cooling ages presently observed in syntaxial bedrock were not present in the syntaxis prior to ca. 4 Ma. Alternatively, the absence of young cooling ages may be explained as dilution of young syntaxial zircons by older zircons from transverse rivers (e.g., the Subansiri or Kameng) upstream of the sampling location, a phenomenon previously observed in the Brahmaputra system by Cina et al. (2009) and Zhang et al. (2012).

In this study, we build on the important work of Chirouze et al. (2013) using new analyses of foreland basin units more proximal to the eastern syntaxis. Specifically, we present new magnetostratigraphy and detrital zircon fission-track and white mica $^{40}Ar/^{39}Ar$ thermochronology from a stratigraphic section located upstream of the transverse Subansiri and Kameng River drainages in Arunachal Pradesh, India. Our fission-track analyses were conducted on zircons for which previously published U-Pb data are available (Lang and Huntington, 2014), permitting a source-specific analysis of low-temperature mineral cooling. Complementary $^{40}Ar/^{39}Ar$ analyses of white mica from the same stratigraphic horizons bolster our interpretations with independent data from a different target mineral that integrates cooling information over longer time scales. We used a one-dimensional thermal model to quantitatively constrain the timing and magnitude of an increase in eastern syntaxial exhumation rate by comparing predicted cooling ages with calculated lag times.

Our results indicate that rapid exhumation has been ongoing within the eastern syntaxis since ca. 5 Ma, following a 5–10-fold increase in the late Miocene exhumation rate. We interpret ~5 m.y. of sustained rapid exhumation as possible evidence for the hypothesized emergence of thermo-mechanical feedbacks (Zeitler et al., 2001). However, this emergence significantly postdates the middle or early Miocene integration of the Yarlung River with the Himalayan foreland (Lang and Huntington, 2014; Bracciali et al., 2015), suggesting that feedbacks did not develop in response to

Geological Society of America Bulletin, published online on 27 April 2016 as doi:10.1130/B31419.1

the proposed capture of the Yarlung River by a smaller Himalayan tributary (Koons, 1995; Brookfield, 1998; Zeitler et al., 2001; Clark et al., 2004). Instead, we suggest that thermomechanical feedbacks may ultimately emerge in areas where large rivers maintain a low-elevation base level and an efficient fluvial system across an area of enhanced rock uplift. Broader comparison of our results with similar studies across the Himalaya demonstrates extraordinary exhumation histories in both syntaxes, potentially resulting from peculiar geodynamics at these orogenic margins.

BACKGROUND

Tectonic and Geomorphic Setting of the Eastern Himalayan Syntaxis

Following the early Eocene end of Tethyan ocean basin subduction, collision between the Indian and Eurasian tectonic plates deformed and uplifted the northern margin of the Indian plate to form the Himalayan orogen (e.g., Gansser, 1964; Searle et al., 1987). Portions of this subducted oceanic lithosphere mark the formal suture zone (called the Indus-Yarlung suture zone) between Transhimalayan intrusive units within Eurasian plate terranes and orogenic units in the Himalaya. The Himalayan orogen is defined along strike by thrust faults that subdivide a sequence of tectonostratigraphic units. The Main Central thrust places deeply exhumed crystalline rocks of the Greater Himalaya above lower-grade metamorphic rocks of the Lesser Himalaya, the Main Boundary thrust places Lesser Himalayan rocks above sedimentary rocks of the Sub-Himalaya, and the Main Frontal thrust places Sub-Himalayan rocks over modern foreland basin alluvium. Greater Himalayan rocks are separated from folded and faulted sedimentary rocks of the Tethyan margin by the South Tibetan detachment system (Fig. 1B; e.g., LeFort, 1975; Yin and Harrison, 2000).

At the eastern margin of the orogen, transition from margin-normal convergence to dextral strike-slip movement warps the suture zone, Himalayan, and Transhimalayan units southward to form the eastern Himalayan syntaxis (e.g., Peltzer and Tapponnier, 1988; Holt et al., 1991; Koons, 1995). Surface topography (Hallet and Molnar, 2001) and geodetic measurements (Sol et al., 2007) illustrate the pattern of lithospheric strain around the margin of the Indian plate indentor (Tapponnier et al., 1990), where the effective lithospheric normal stress is reduced and minor deviations may result in enhanced lithospheric strain (Enlow and Koons, 1998), priming the region for dynamic modification by surface processes (Simpson, 2004).

Within the eastern syntaxis, an active crustal-scale antiform (Burg et al., 1998) or pop-up structure (Ding et al., 2001) called the Namche Barwa metamorphic massif is deeply incised along a rapidly eroding reach of the Yarlung River. After flowing >1000 km along the suture zone in southeastern Tibet, the Yarlung River drops over 2 km through a narrow (Montgomery, 2004) bedrock gorge often referred to as the "Tsangpo Gorge." Within the gorge, erosion rates (Stewart et al., 2008; Enkelmann et al., 2011), proxies for fluvial incision (Finlayson et al., 2002; Finnegan et al., 2008), and local topographic relief (Larsen and Montgomery, 2012; Korup et al., 2010) dramatically increase to define one of the most dynamic landscapes on Earth (Zeitler et al., 2001).

Extensive bedrock thermochronology documents rapid late Pliocene and Pleistocene exhumation rates (5–10 km/m.y.) focused around the massif. Zircon fission-track data, which reflect cooling from shallow crustal temperatures of ~230 °C (Brandon and Vance, 1992), are younger than 3.5 Ma within the massif, and younger than 1 Ma within the Tsangpo Gorge specifically (Burg et al., 1998; Seward and Burg, 2008; Zeitler et al., 2014). Biotite $^{40}Ar/^{39}Ar$ cooling ages, which reflect cooling from higher temperatures (>300 °C for such rapid cooling rates; Dodson, 1973; McDougall and Harrison, 1999), also are less than 1 Ma in samples collected along the Tsangpo Gorge but rapidly increase with distance from the core of the massif (Fig. 1B; data from Ding et al., 2001; Malloy, 2004; Geng et al., 2006; Zeitler et al., 2014). Zircon U-Pb geochronology from bedrock samples within the gorge further indicates that local anatexis was associated with rapid rock exhumation in the Pliocene, and potentially the late Miocene (Ding et al., 2001; Booth et al., 2004, 2009). Recent modeling of this extensive suite of bedrock cooling ages predicts a pulse of rapid exhumation in the late Miocene between 5 and 10 Ma (Zeitler et al., 2014). We test this prediction with additional analysis of detrital minerals preserved in the proximal sedimentary record.

We predict that the appearance of young (relative to depositional age) detrital cooling ages in proximal foreland basin units may be evidence for earlier exhumation of the Namche Barwa massif, provided a complementary diagnosis of sediment provenance. Erosion of the Namche Barwa massif presently enriches downstream river sediment in rapidly cooled minerals from massif bedrock, adding a characteristic young cooling age component to detrital zircon ages that represents as much as 45% of zircons entering the Himalayan foreland basin (e.g., Pik et al., 2005; Stewart et al., 2008; Enkelmann et al., 2011; Lang et al., 2013). Foreland basin units proximal to the eastern syntaxis contain evidence of a drainage system encompassing both Himalayan and Tibetan source terranes throughout their depositional history (e.g., Cina et al., 2009; Lang and Huntington, 2014), and an integrated Yarlung-Siang-Brahmaputra river system may have similarly carried rapidly cooled minerals into the foreland basin once rapid exhumation of the massif began. The presence of Himalayan and Tibetan detritus in proximal foreland basin units further indicates that if the Yarlung River integrated with the Siang-Brahmaputra system by river capture, this event must have occurred prior to foreland basin deposition. Thus, evidence for earlier massif exhumation emerging within these units postdates river integration and may not be directly related to a capture event.

Easternmost Himalayan Foreland Basin

The Himalayan foreland basin is peripheral to the mountain front and nearly continuous along the Himalayan arc (Beaumont, 1981; Najman, 2006). Near its eastern limit, the basin is less than 100 km wide, narrowly confined between active thrust faults: the Main Frontal thrust to the northwest, Mishmi thrust to the northeast, and Naga thrust to the southeast. The total thickness of Cenozoic sedimentary units within the basin may be as much as 7 km (Mathur and Evans, 1964; Karunakaran and Ranga Rao, 1976), and basin thickness increases toward the Himalayan mountain front (Verma and Mukhopadhyay, 1977). Neogene units are uplifted by the Tipi thrust and Main Frontal thrust to form steep foothills at the mountain front. These units are locally offset by smaller crosscutting faults (e.g., Agarwal et al., 1991; Yin et al., 2010; Burgess et al., 2012) but remain traceable along strike of the mountain front from the eastern syntaxis westward into Bhutan (Fig. 1B; Ranga Rao, 1983; Kumar, 1997).

Sedimentary rocks exposed in these foothills are traditionally divided into three lithologically distinct units (e.g., Karunakaran and Ranga Rao, 1976; Bhareli and Ratnam, 1978; Yin, 2006) and correlated with the more extensively studied Siwalik Group in the central and western Himalaya (e.g., Kumar, 1997; Chirouze et al., 2012a,b). Although these units are locally called the Kimin, Subansiri, and Dafla formations (Kumar, 1997), we adopt the corresponding Upper, Middle, and Lower Siwalik Formation nomenclature for consistency with the well-established, broader Himalayan literature (e.g.,

Geological Society of America Bulletin, published online on 27 April 2016 as doi:10.1130/B31419.1

Pilgrim, 1913) and previous work from the same location (Lang and Huntington, 2014). In this study, we specifically focus on detailed observations along the Siji River near the village of Likabali, including locations previously sampled by Lang and Huntington (2014).

Regionally, these units comprise an upward-coarsening clastic sedimentary sequence resting unconformably on metasedimentary units of the Gondwana formation. The Lower Siwalik Formation is characterized by compact interbedded sandstone and shale; the Middle Siwalik Formation is a softer and coarser micaceous, concretionary sandstone; and the Upper Siwalik Formation is characterized by interbedded conglomerate, sandstone, and mudstone (e.g., Ranga Rao, 1983; Kumar, 1997; Chirouze et al., 2012a). A gradational contact between the Upper and Middle Siwaliks is preserved in many Siwalik sections (e.g., Jain et al., 1974; Chirouze et al., 2012a), whereas the Lower Siwalik is commonly placed structurally above these units on the Tipi thrust (e.g., Agarwal et al., 1991; Yin et al., 2010; Burgess et al., 2012).

Constraints on Depositional Age

Depositional ages of eastern Siwalik units are poorly constrained. Biostratigraphic constraint comes from a single mammalian fossil specimen (*Bos* sp.) from a conglomeratic bed of the Upper Siwalik (Singh, 1975, 1976). This solitary observation corroborates an informal description of a similar fossil by Maclaren (1904) observed north of the Subansiri River to loosely indicate a Pleistocene depositional age for the Upper Siwalik. Arenaceous foraminifera (specifically *Trocommina* sp.; Ranga Rao, 1983), megafloral assemblages including *Zizyphus* sp. and *Sigigium* sp. (Singh and Prakash, 1980), and palynofossil suites (Dutta, 1980) observed in the Lower Siwalik suggest an early or middle Miocene depositional age for this unit (Singh and Tripathi, 1989; Singh, 1999).

The most robust depositional age constraints for these units come from a combination of detrital thermochronology and magnetostratigraphy (Chirouze et al., 2012a). This work brackets the depositional age for the Upper-Middle Siwalik contact between 2 and 3 Ma and the Middle-Lower Siwalik contact between 11 and 13.5 Ma in a section along the Kameng River near Bhalukpong. Chirouze et al. estimated that the average sediment accumulation rate varies in this location between 420 and 440 m/m.y., which is higher than correlated sections from the central and western Himalaya (e.g., Johnson et al., 1985; Gautam and Fujiwara, 2000; Ojha et al., 2009).

Constraints on Sedimentary Provenance

Siwalik units across the Himalayan foreland are broadly interpreted to be synorogenic deposits of Himalayan detritus eroded during periods of late Cenozoic thrusting (e.g., Heim and Gansser, 1939; DeCelles et al., 1998; Najman, 2006). Paleocurrent indicators from easternmost exposures of Middle and Upper Siwalik Formations show that flow direction varied (Chirouze et al., 2013) but was dominantly to the south or southwest from a northern source region (e.g., Jain et al., 1974; Cina et al., 2009; Kesari, 2010; Chirouze et al., 2012a) with no indication of flow reversal during deposition of the sequence.

Modal analyses are consistent with a northern source in both Himalayan and Tibetan terranes. Framework grains (e.g., Gogoi, 1989; Baruah, 2001) are characteristic of a recycled orogenic provenance, and heavy mineral suites indicate contributions from plutonic and metamorphic sources. Specifically, tourmaline, epidote, zircon, rutile, hornblende, garnet, staurolite, and kyanite metamorphic index minerals are found in all units, with andalusite and sillimanite appearing in the Upper Siwalik Formation (Singh, 1976; Singh et al., 1982; Ranga Rao, 1983).

Detrital zircon U-Pb geochronology from five sections in eastern Siwalik units (Cina et al., 2009; Lang and Huntington, 2014) indicates a mixed Tibetan and Himalayan provenance. Specifically, the presence of Gangdese-age zircons (Stewart et al., 2008; Cina et al., 2009; Zhang et al., 2012) in all Siwalik samples north of Bhalukpong (see Fig. 1B) demonstrates that Tibetan source areas presently west of the Namche Barwa massif were included in the contributing area to the foreland basin. This observation was interpreted by Lang and Huntington (2014) to represent a fluvial connection maintained through the eastern syntaxis since at least the middle and possibly early Miocene. Bulk ε_{Nd} and ε_{Hf} isotopic analyses indicate that the absence of Gangdese-derived detritus in the Lower Siwalik near Bhalukpong may be explained by local deposition from a transverse Himalayan river like the Kameng River (Chirouze et al., 2013).

METHODS

Mapping and Stratigraphic Surveying

To identify faulting and other potential complications in our interpretation of Siwalik stratigraphy, we mapped the Siji River area with a focus on Upper and Middle Siwalik exposures. Accessibility in the area is severely restricted, and exposure is limited to river channels at low-flow conditions, road cuts, and landslide scars. Because of inaccessibility, mapping and stratigraphic surveying focused on traverses along the Siji River and adjacent tributaries. Bedding measurements and unit contacts were plotted in the field on 1:12,000 scale satellite images, and contacts were extrapolated away from the direct observations along strike of topographic dip slopes measured using Google Earth.

Stratigraphic surveying of the Upper and Middle Siwalik Formations using a 1.5 m Jacob's staff and Abney level progressed up section along the Siji River from the mountain front near Likabali to the Tipi thrust near Siji village. Surveying included observations of bed thickness, grain size, sedimentary structures, and clast lithology in channel lag deposits and conglomerate beds.

Magnetic Susceptibility and Magnetostratigraphy

We collected one to three oriented block samples for analysis of paleomagnetic polarity every 20 m in the lower 1.6 km of the Middle Siwalik. Every 100 m, we collected 3–6 samples for replicate analysis from single bedding horizons. Block samples were cored, cut into specimens, and analyzed at the Pacific Northwest Paleomagnetism Laboratory at Western Washington University. All subsequent processing was conducted in a magnetic field–free room. The specimens were first analyzed using an AGICO KLY3-S Magnetic Susceptibility Bridge to determine their anisotropy of magnetic susceptibility. In clastic sediments, the plane of maximum susceptibility is commonly tilted from horizontal due to imbrication of grains in the rock, and this imbrication is a useful supplement to field measurement of paleocurrent direction (e.g., Novak et al., 2014). To determine paleomagnetic polarity, we measured the remanent magnetization of 126 specimens from 79 sites spanning the lower 1.6 km of the Middle Siwalik. Measurements were made using a 2-G Enterprises 755 superconducting rock magnetometer with 0.001 mA/m sensitivity. Thermal demagnetization in an ASC Model TD48 oven began with closely spaced temperature steps on a subset of specimens to determine optimal step spacing. This was followed for the rest of the specimens by demagnetization in seven 70 °C to 100 °C temperature steps from ~180 °C to 580 °C. Magnetic susceptibility was measured on a Bartington MS2 susceptometer after specific temperatures to monitor changes in magnetic mineralogy. Standard analytical methods were used to identify, quantify, and analyze remanent magnetization components and interpret original polarity.

Geological Society of America Bulletin, published online on 27 April 2016 as doi:10.1130/B31419.1

Detrital Thermochronology

To interpret changes in source exhumation rates, we analyzed detrital mineral cooling ages from sampled stratigraphic horizons and from the modern Siang River and adjoining Himalayan tributaries. We collected five samples from the Upper and Middle Siwalik Formations in the Tipi thrust footwall for zircon fission-track and white mica $^{40}Ar/^{39}Ar$ thermochronology. Fission-track analyses of modern sediments from the Siang River and adjoining Himalayan tributaries have been previously published (Stewart et al., 2008; Enkelmann et al., 2011), and we collected an additional six samples of modern sediment from the same locations for white mica $^{40}Ar/^{39}Ar$ analyses (sample locations in Fig. 1B). Combining multiple thermochronological data sets from the same stratigraphic horizons permits a robust interpretation of exhumation rate changes that may identify potential biases in cooling age distributions from mineral heterogeneity in the source region (e.g., Avdeev et al., 2011).

Preparation of sediment and sedimentary rock samples started with manual disaggregation in a dilute (<3%) HCl solution. Resulting grains were wet-sieved to isolate the 63–250 mm, 250–500 mm, and 500–1000 mm grain-size fractions. For both zircon and white mica samples, we analyzed at least 50 grains per sample (a total of 1084 grains distributed among 11 sample locations) to be at least 95% confident that our analyses did not miss an age component greater than 10% of the true age distribution (Vermeesch, 2004).

White Mica $^{40}Ar/^{39}Ar$ Analysis

Optically pure (inclusion-free) grains of white mica were hand selected from the 500–1000 mm grain-size fraction (also the 250–500 mm fraction for the Kapu sample to evaluate potential size-age bias), cleaned in acetone, methanol, and deionized water, placed in aluminum foil packages and shielded with Cd for fast neutron irradiation. The packages were irradiated for 0.5 and 6.1 h in the 5C core and medium-flux positions at the McMaster University nuclear reactor in Hamilton, Ontario, Canada. Biotite age standard HD-B1 (24.18 Ma; Schwarz and Trieloff, 2007) was used to monitor the neutron flux gradient along with Kalsilite ($KAlSiO_4$) and CaF_2 salts to determine interfering nuclear production ratios.

Single-grain, total fusion $^{40}Ar/^{39}Ar$ analyses were conducted at the Arizona State University Noble Gas Geochronology and Geochemistry laboratory using a high-sensitivity Nu Instruments Noblesse multicollector mass spectrometer with Nier-type source and zoom optics, coupled to a 60 W IPG Photonics 970 nm diode laser with Photon Machine optics linked to a Newport controller. Age standard and unknown single-grain samples were kept at 120 °C in an ultrahigh-vacuum chamber for 1 d and then turbo pumped for 1 d to remove adsorbed atmospheric argon from the samples and chamber walls.

Total grain fusion was accomplished by firing the laser at 15 W for 120 s with a 0.6 mm beam diameter; the beam was moved to completely fuse each grain. Gases released by laser heating were cleaned in SAES NP10 getter pumps at 400 °C and room temperature to remove active gases. Ar isotopes were measured on one Faraday detector fitted with a 10^{11} Ohm resistor and one ETP ion-counting multiplier detector calibrated with air pipette shots. Automation of the analytical system was controlled by the Mass Spec software program.

Ages were calculated from isotopic ratios and *J* values using the Isoplot software plug-in for Microsoft Excel and the decay constant, branching ratio, and atmospheric Ar ratios from Steiger and Jäger (1977).

Zircon Fission-Track Analysis

Fission tracks were analyzed at Apatite to Zircon, Inc., using the laser ablation–inductively coupled plasma–mass spectrometry (LA-ICP-MS) methods of Donelick et al. (2005) and Chew and Donelick (2012). Zircons used for fission-track analysis were originally separated for U-Pb analysis by Lang and Huntington (2014) from the 63–250 mm grain-size fraction with standard magnetic and density separation techniques. Prior to analysis, zircons from each sample were mounted in Teflon, polished to expose internal grain surfaces, and imaged with cathodoluminescence and high-resolution electron backscattering (see Lang and Huntington, 2014).

For fission-track analysis, one grain mount per sample was etched in a NaOH-KOH eutectic melt at ~230 °C for a single duration lasting 24–72 h. Etching time varied to ensure an adequate number of suitably etched grains on a single mount. Fission tracks were counted from within each ~30-mm-diameter laser ablation pit at 1562.5× dry magnification in unpolarized, transmitted, and reflected light on a Nikon Optiphot 2 microscope. The LA-ICP-MS approach uses a modified zeta calibration (Hurford and Green, 1983; Hasebe et al., 2004) in which zeta calibration standards from Fish Canyon Tuff were updated during each LA-ICP-MS session and smoothed using a load-specific running median. U, Th, and Sm abundances were determined by LA-ICP-MS using an Agilent 7700x quadrupole mass spectrometer coupled to a Resolnetics RESOlution M-50 193 nm excimer laser.

RESULTS

Stratigraphy of the Siji River Region

We focused stratigraphic surveying and sampling across the gradational Upper and Middle Siwalik contact exposed in the footwall of the Tipi thrust (Fig. 2). Exposures of the Lower Siwalik are faulted out of stratigraphic position and internally deformed (Jain et al., 1974; Agarwal et al., 1991). Determination of stratigraphic position within the Lower Siwalik would have required extensive additional magnetostratigraphy, which was impractical due to the severely restricted exposure. In contrast, the Upper and Middle Siwaliks are complete and well exposed in the Siji River and adjoining tributaries. In this region, coarse sandstones of the Middle Siwalik grade up section into interbedded siltstone and conglomerate of the Upper Siwalik. For correlation of this contact with other Siwalik sections, we defined the base of the Upper Siwalik to be where the abundance of siltstone beds abruptly increases (Fig. 3).

Middle Siwalik

The Middle Siwalik is at least 3.2 km thick in the Siji River region (Fig. 3). Resistant beds support relatively high topography with steep slopes commonly following bedding planes. This unit is defined by thin to very thick beds of monotonous sandstone that coarsen upward from fine- to very coarse-grained sand with interbedded gravel and cobble conglomerate.

The lower 1.7 km of the unit are distinguished by the down-section reduction and eventual absence of quartzite, metamorphic and volcanic clasts in channel deposits; and reductions in grain size, characteristic bed-form scale, and concentration of large, visible mica grains. This lower portion of the unit contains thin to thick beds of very fine- to medium-grained sandstone with rare beds of matrix-supported conglomerate. Sandstone beds exhibit a variety of stratification at centimeter to meter scales, including climbing ripples, planar bedding, and trough cross-bedding. Many beds exhibit truncated fining-upward sequences. Sand grains are angular to subangular and range from poorly to well sorted. In the lowest horizons, interbedded matrix-supported conglomerate contains angular to subangular clasts of hard red or gray siltstone, mudstone, and coal. Decimeter- to meter-scale round and tabular concretions are concentrated along bedding planes and surround coal fragments. Detrital coal fragments are ubiquitous, and whole logs

Geological Society of America Bulletin, published online on 27 April 2016 as doi:10.1130/B31419.1

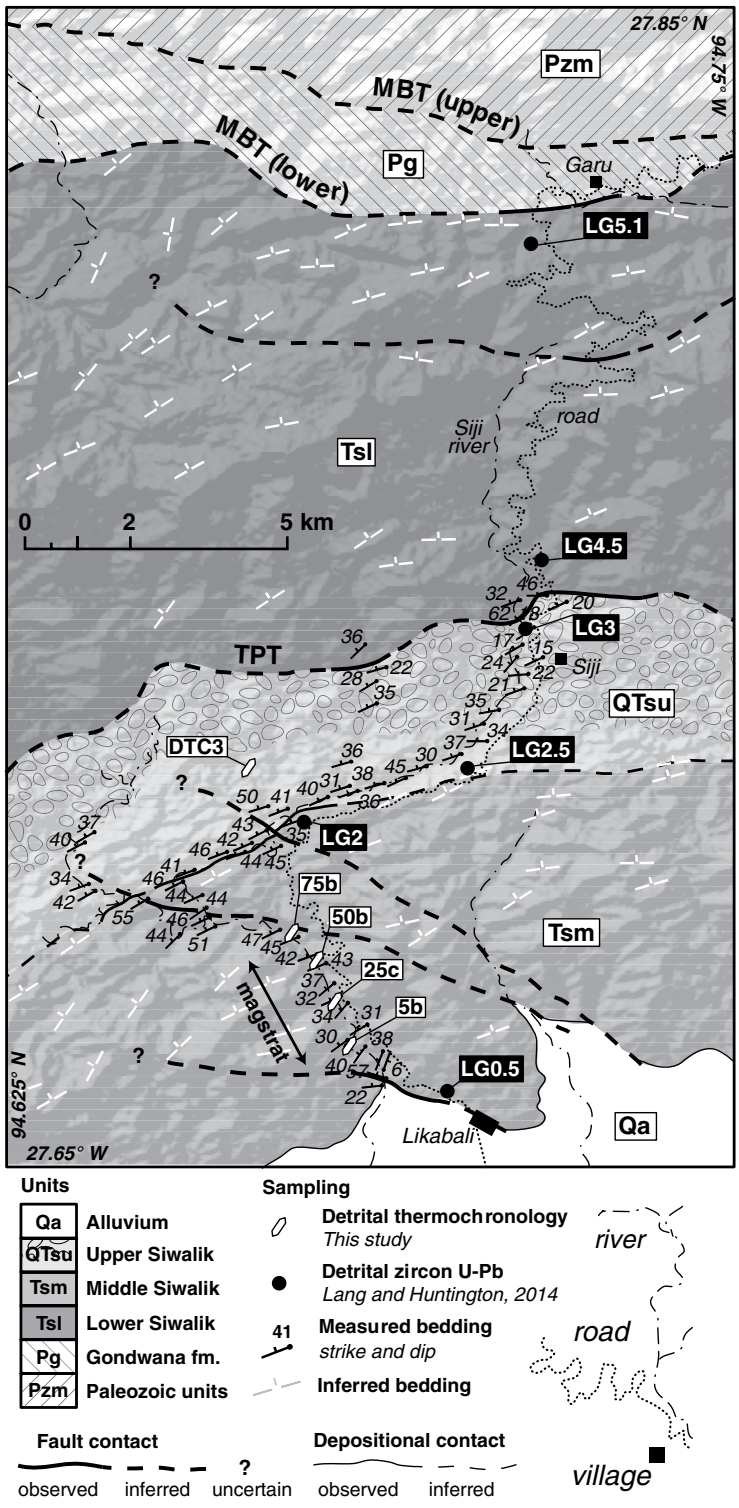

Figure 2. Geologic map of the Siji River area. Bedding symbols follow a sampling transect through the Upper and Middle Siwalik. Northwest-southeast–striking faults do not disrupt the portion of the section sampled for magnetostratigraphy. Boulder pattern depicts approximate extent of growth strata in the Upper Siwalik (see text for discussion). Sample localities include additional detrital zircon U-Pb samples from Lang and Huntington (2014) with samples from this study. Structure abbreviations: MBT—Main Boundary thrust; TPT—Tipi thrust.

and stumps are observed throughout this portion of the unit.

The upper 1.5 km of the unit are distinguished by very thickly bedded, coarse- to very coarse-grained sandstone, less common matrix and clast-supported conglomerate, and rare siltstone and mudstone beds. Sandstones coarsen upward from coarse to very coarse grained in the uppermost 800 m of the unit. Sandstones are generally massive or exhibit faint cross-bedding at meter scales or larger; some contain pebble-gravel channel deposits with increasing abundance in the upper portion of the unit. Grains are angular to subangular and poorly to moderately sorted. Sandstones are micaceous, with large micas observed in very coarse-grained horizons. Channel deposits first appear as discontinuous stringers but progressively thicken up section into thick lenticular beds of matrix and clast-supported conglomerate. These deposits contain clasts of siltstone, coal, variously colored quartzite, vein quartz, volcanic breccia, amygdular and vesicular basalt, orthogneiss, and schist. These clast lithologies are characteristic of Lesser Himalayan units exposed in the Siang valley. Volcanic rocks are rarely observed in Lesser Himalayan units and may be sourced specifically from the Abor volcanics, which are exposed within the immediate vicinity of the Siang River (Jain and Thakur, 1978; Ali et al., 2012). This part of the Middle Siwalik also contains centimeter- to meter-scale round and tabular concretions, commonly distributed along bedding planes. Coal logs, stumps, and large coal fragments are observed throughout this portion of the section, as well as thick beds of laminated gray siltstone. Green-brown claystone is rarely observed.

Upper Siwalik

The Upper Siwalik is at least 1.5 km thick in the Siji River region. Relative to the Middle and Lower Siwalik Formations, the unit is recessive and forms more subdued topography. The angular path of the Siji River may result from exploitation of easily eroded silt beds in the lower portion of the unit before the river crosses the Middle Siwalik to enter the Brahmaputra braid plain.

The lower 900 m of the Upper Siwalik are characterized by discontinuous sequences of thickly to very thickly interbedded conglomerate, sandstone, and siltstone. Gravel-cobble conglomerate is clast supported and typically massive or crudely cross-bedded. Conglomerate clasts are moderately sorted, subangular to subrounded, and contain similar lithologies as observed in channel deposits of the Middle Siwalik. Siltstone clasts are commonly angular and may have been scoured from silt beds

Geological Society of America Bulletin, published online on 27 April 2016 as doi:10.1130/B31419.1

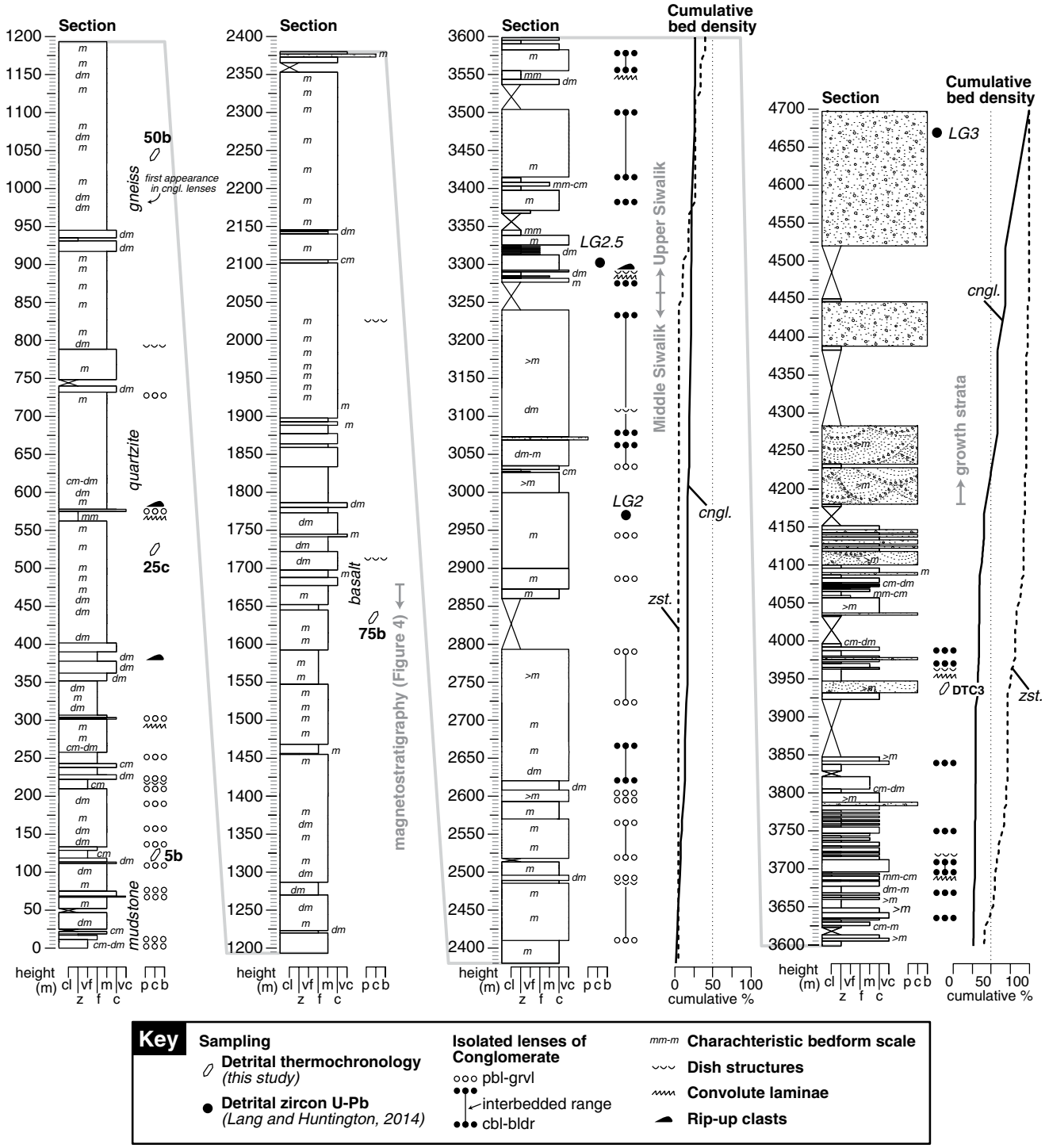

Figure 3. Stratigraphic section of Upper and Middle Siwalik units exposed in the Tipi thrust footwall. Observations of the Middle Siwalik are consistent with a vertically stacked fluvial architecture similar to the modern Brahmaputra River. Sandstone (vf—very fine, f—fine, m—medium, c—coarse, vc—very coarse), siltstone (z—silt, cl—clay), and conglomerate (p—pebble, c—cobble, b—boulder) beds coarsen upward with an increase in charachteristic bed-form scale (m—meter, dm—decimeter, cm—centimeter, mm—millimeter). Isolated conglomerate lenses also coarsen upward and are first dominated by angular, locally derived mudstone clasts, followed by the appearance of quartzite, gneiss, and basaltic clasts that may indicate detritus from source rocks exposed along the Siang River. The base of the Upper Siwalik is defined where the density of siltstone beds increases. Thick siltstone beds also exhibit evidence of dewatering after rapid deposition. Very thick, highly oxidized conglomerate in the upper ~500 m of the section is interpreted as growth strata based on decreasing bed dip with proximity to the Tipi thrust. The stratigraphic positions of samples from this study and additional samples from Lang and Huntington (2014) are indicated.

Geological Society of America Bulletin, published online on 27 April 2016 as doi:10.1130/B31419.1

within the unit. Sandstones are medium to very coarse grained and exhibit decimeter- to meter-scale cross-bedding, parallel bedding, or no bed forms. Siltstone and very fine-grained sandstone beds exhibit parallel lamination, cross lamination, and postdepositional dewatering and soft sediment deformation structures (e.g., dish structures, convolute lamination). Beds of both sandstone and siltstone are micaceous, and some contain very coarse mica grains. Large stumps and logs occur in this portion of the unit.

In the upper 600 m of the unit, the proportion of conglomerate beds increases at the expense of medium- and coarse-grained sandstone and siltstone beds, which are reduced to discontinuous lenses within conglomerate beds. Clast-supported conglomerates are strongly oxidized and loosely consolidated in this portion of the section. Clasts are moderately to well sorted, subangular to subrounded, and subtly coarsen upward from cobbles to boulders. Beds are typically massive, but some are crudely cross-bedded. Clasts also are crudely imbricated, reflecting a dominantly south-southeastern flow direction (consistent with observations of Jain et al., 1974) or showing no preferential flow direction. Clasts are dominated by red, green, white, and gray quartzite with some basalt, gneissic metamorphic rocks, dolomite, and rare coal fragments. We note that the dip of the uppermost conglomerate beds decreases with proximity to the Tipi thrust, indicating that these strata may have been deposited during tilting of underlying units (i.e., growth strata). Growth strata also have been observed in the uppermost Upper Siwalik near Bhalukpong (Burgess et al., 2012).

Interpretation of Depositional Environment

Our observations are consistent with previous interpretations of primarily alluvial deposition for Upper and Middle Siwalik Formations in this region (e.g., Karunakaran and Ranga Rao, 1976; Ranga Rao, 1983; Kumar, 1997; Chirouze et al., 2012a). Specifically, the abundance of large-scale characteristic fluvial bed forms in the Middle Siwalik indicates deposition by a large, braided sand-bed river (Bristow and Best, 1993; Miall, 1996). Overlapping channel deposits with truncated fining-upward sequences indicate a vertically stacked fluvial architecture (Walker and Cant, 1984) characteristic of axial deposition in a basin similar to the present Brahmaputra River.

Considering this interpretation of the depositional environment, the up-section increase in grain size and characteristic bed-form scale within the Middle Siwalik may indicate increasing flow velocity (Middleton and Southard, 1984; van Rijn, 1984) and depth (Yalin, 1972), or sediment discharge (Gilbert, 1914; Karim and Kennedy, 1990), rather than additional input of coarse sediment from transverse Himalayan rivers at the axial river margin. Unfortunately, truncation of existing bed forms in this portion of the section complicates a detailed interpretation of paleocurrent direction in the field. However, analysis of magnetic susceptibility anisotropy is consistent with a southwest paleocurrent direction (see details in Magnetostratigraphy section of Results).

We interpret the increased proportion of gravel-cobble conglomerate and siltstone beds across the Upper-Middle Siwalik contact to mark increased contribution from transverse Himalayan rivers. This interpretation is consistent with the bulk isotopic measurements of Chirouze et al. (2013), which indicate a local Himalayan provenance in the Upper Siwalik near Bhalukpong. Moreover, movement of the Tipi thrust since ca. 1 Ma (Chirouze et al., 2013) may explain the decreasing dip of depositional surfaces in the uppermost portion of the Upper Siwalik as growth strata were deposited concurrently with tilting of underlying Siwalik units. Importantly, evidence of growth strata is only observed directly within the uppermost Upper Siwalik. This indicates that recycling of detrital minerals with older cooling ages from lower Siwalik units may have been a potential source for the Upper Siwalik sample (DTC3), but not also for the Middle Siwalik samples.

The increased contribution of gravel and cobble conglomerate in the Upper Siwalik has been explained as a consequence of erosional unroofing of the Himalaya during the onset of glaciation in the late Cenozoic (Burbank, 1992). Although the eastern Himalayan foreland is more narrowly confined than the central and western portions of the foreland, we consider that this hypothesis may be equally valid to explain the abrupt change in grain size between the Middle and Upper Siwalik Formations. Glaciation may have also changed the characteristic grain-size distribution of eroded Himalayan detritus (Goldthwait, 1971), supplying both more silt and more gravel to the foreland. Previous researchers have proposed that glaciation of the eastern Himalayan syntaxis resulted in episodic damming and outburst flooding (e.g., Montgomery et al., 2004; Lang et al., 2013), which we suggest may have also influenced Upper Siwalik sedimentation. We speculate that thick siltstones and fine sandstones interbedded with conglomerate in the lower portion of the Upper Siwalik may represent deposition from episodic glacial outburst floods debouching into the foreland basin. Many siltstone and fine sandstone beds cap fining-upward sequences that include characteristic dewatering structures indicative of rapid deposition of hyperconcentrated floodwaters (Benvenuti and Martini, 2002). More detailed analyses of the detrital provenance of these specific beds would test this speculative interpretation and potentially provide new insight into the impact of such rare yet geomorphically significant events (Lang et al., 2013).

Structure of the Siji River Region

We mapped the Siji River area at a larger scale than previously published maps (e.g., Jain et al., 1974; Agarwal et al., 1991) to determine the best location for stratigraphic surveying (Fig. 2). Near the northern margin of the study area, the Main Boundary thrust places Paleozoic units including the Permian Gondwana units structurally above the Lower Siwalik, forming a distinctive topographic break. The Lower Siwalik is internally deformed, with potentially antithetic reverse faulting observed in outcrops along the Likabali-Garu road. This internal deformation combined with poor exposure prohibits accurate assessment of Lower Siwalik thickness, which has been previously estimated to be ~2 km in this location (Jain et al., 1974). The Tipi thrust places the Lower Siwalik structurally above the Upper Siwalik. This relationship is directly observed in the Siji River near Siji village and may be traced in the topography due to the contrasting unit competence. A complete section of Upper and Middle Siwalik units most appropriate for measurement is observed along the mountain front where the Main Frontal thrust places these units structurally above Quaternary alluvium.

The gradational Upper-Middle Siwalik contact is locally displaced in a left-lateral sense by several west-northwest– to east-southeast–striking faults. These faults may also extend southeastward to the trace of the Main Frontal thrust at the mountain front, where Misra and Srivastava (2009) have suggested that young fluvial terraces near Likabali may result from recent fault activity. The northwestern tips of the faults do not obviously cut the Tipi thrust but may be buried by growth strata in the uppermost portion of the unit. Left-lateral displacement on these west-southwest– to east-southeast–striking faults may be consistent with reverse-sense slip, but without more detailed observations, it is difficult to quantify the total amount and orientation of slip. Regardless, these structures do not exhibit sufficient displacement to confound stratigraphic or magnetostratigraphic interpretations.

Magnetostratigraphy

We measured the characteristic remanent magnetization of 126 specimens from 79 samples collected through the lower 1.7 km of our surveyed transect (Fig. 4). The characteristic remanent magnetization of a sample specimen is interpreted to represent original polarity of the magnetic field during deposition of detrital minerals, although subsequent magnetic overprints may complicate this interpretation. Characteristic remanent magnetization is defined during step-wise thermal demagnetization as the natural remanent magnetization component is removed over the highest-temperature demagnetization steps. Above ~500 °C, demagnetization paths clearly trend toward the origin, and it is possible to distinguish between the higher-temperature characteristic components and lower-temperature overprints. Figure 4A shows examples of specimens with clearly distinguishable normal and reversed polarity demagnetization paths corrected for bed tilt plotted on orthogonal diagrams. Distinguishing between original and overprint components, however, is difficult in samples for which the natural remanent magnetization is less well defined at high temperatures.

For many of our specimens, characteristic remanent magnetizations were difficult to clearly resolve. Those specimens displayed erratic changes in magnetization strength and direction and a marked increase in magnetic susceptibility above 250 °C. This behavior is consistent with the growth of magnetite, a phenomenon previously observed in eastern Himalayan Siwalik samples (Chirouze et al., 2012a). Instrument noise is not a confounding factor, because it was at least an order of magnitude less than the specimens' magnetic moments prior to onset of erratic behavior, nor was the behavior due to physical disintegration of samples, as only a few of the coarsest-grained specimens disintegrated before the onset of erratic behavior.

Traditionally, classification of magnetic polarity zones used for a polarity time-scale correlation is based on distribution of virtual geomagnetic poles (VGP). However, VGPs could not be calculated for most specimens because their characteristic remanence could not be fit well to a vector component. We instead classified polarity zones by individually evaluating the trend of demagnetization paths on orthogonal and equal-area plots to determine the polarity tendency. Polarity tendency is defined as the angle between a normal polarity reference direction (359.5° declination and 46.7° inclination) and directions from least squares free-line regressions to low-, medium-, and high-temperature measurements. A tendency of the demagnetization path toward a normal direction would decrease this angle, whereas a

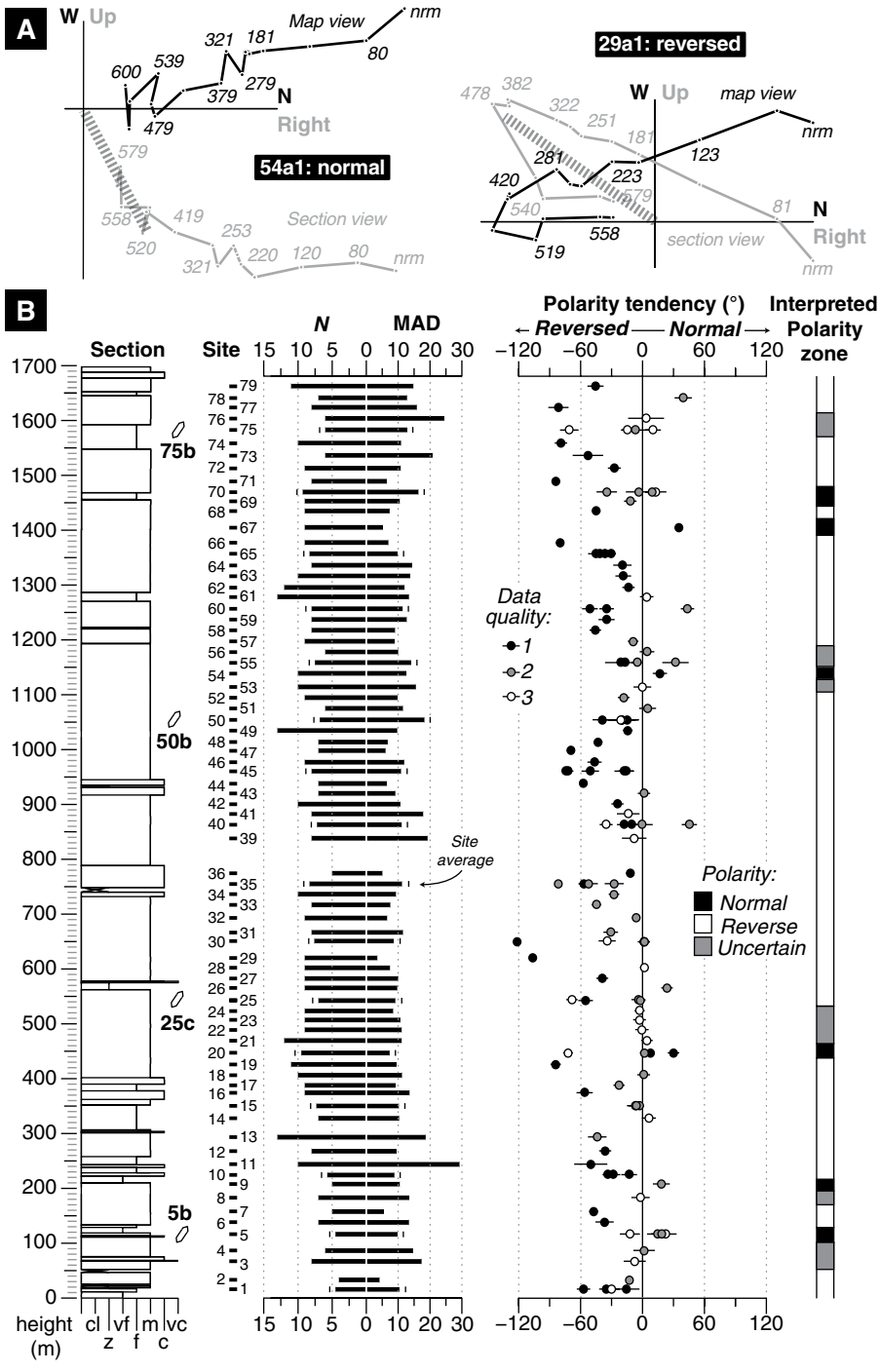

Figure 4. (A) Examples of demagnetization paths for normal (54a1) and reversed (29a2) polarity specimens. Plots are horizontal (map view) and vertical plane (section view) orthogonal projections. Respective temperature steps are labeled (in °C) for each natural remanent magnetism (nrm) position plotted. The highest-temperature segments are interpreted to be original magnetizations (thick dashed line through origin). (B). Magnetostratigraphy of the lower Middle Siwalik unit (grain size classified as in Fig. 3). We analyzed 79 sites, determining polarity to be normal, reverse, or uncertain by individual inspection of demagnetization paths and calculation of polarity tendency. See text for discussion of data quality and precision. *N*—number of specimen measurements per sample; and MAD—maximum angular deviation (Kirschvink, 1980). For sites with multiple samples, averages for *N* and MAD are indicted with tick marks.

Geological Society of America Bulletin, published online on 27 April 2016 as doi:10.1130/B31419.1

tendency of the demagnetization path toward a reversed direction would increase this angle. We estimated the precision of polarity tendency as the maximum angular deviation of each regression (Kirschvink, 1980).

Low- and medium-temperature measurements have a mean declination of 1.7° and inclination of 43.8° (with a 3.3° 95% confidence interval). This direction is statistically indistinguishable from the present axial dipole field (0° declination and 43.6° inclination), indicating that the low-temperature overprints were acquired after tilting of the strata.

We classified higher-temperature measurements, which varied in data quality, into three groups. First-quality data have distinct normal or reverse polarity tendency (i.e., demagnetization paths trend clearly toward normal or reverse reference directions). Second-quality data are more ambiguous due to short or noisy demagnetization paths. Third-quality data are most ambiguous because higher-temperature measurements were not clearly differentiable from a posttilting overprint. All measurements, interpretation, and polarity determination are reported in the Data Repository.[1]

Correlation to Geomagnetic Polarity Time Scale

We used specimen polarity tendency measurements to delineate 20 zones with normal or reversed polarity and zones where polarity was uncertain (Fig. 4B). We assume that all polarity zones may be correlated to chrons younger than the long-duration normal C5n.2n chron between 9.9 and 11.0 Ma (Gradstein et al., 2012) because our observations did not indicate any evidence for normal polarity or potentially normal polarity zones thicker than ~100 m. The long normal C5n.2n chron should constitute a >370-m-thick region, provided accumulation rates typical of the central and eastern Himalaya (Ojha et al., 2000, 2009; Chirouze et al., 2012a), and thus it is apparently missing from this section.

We correlated our polarity zone sequence from our section to the *2012 Geomagnetic Polarity Timescale* (Gradstein et al., 2012) using Cupydon, an iterative method based on the Dynamic Time Warping algorithm (Lallier et al., 2013). This method iteratively compares permutations of our polarity sequence to this time-scale reference ranging from C1n to C5n.1, ranking correlations by fit. Correlation fit is determined by minimizing the local variability in accumulation rate, such that the best-fit correlation has the lowest local variability. The algorithm further allows for chrons to be skipped over a five-zone range in the polarity zone sequence. Results illustrate a best-fit correlation between the C2Ar chron at 3.5 Ma and C4n.1r chron at 7.6 Ma (Fig. 5A). This correlation indicates an average accumulation rate of 403 m/m.y. (Fig. 5B), which is slightly less than rates previously reported in the central and eastern Himalaya (Ojha et al., 2009; Chirouze et al., 2012b). Chirouze et al. (2012a) independently made a similar correlation in a Middle Siwalik section from the Tipi thrust footwall along the Kameng River, also lacking the long normal C5n.2n chron and contained similar trends in grain size and bed thickness (Fig. 5A).

We estimated the depositional ages of Middle Siwalik horizons sampled for detrital thermochronology by linear interpolation between matched chrons. The depositional age for the single Upper Siwalik sample (DTC3) was not constrained by magnetostratigraphy, and we tentatively estimate the depositional age for this sample between ca. 1 and 2 Ma based on its stratigraphic position beneath the appearance of growth strata related to movement along local faults since ca. 1 Ma (Chirouze et al., 2013).

Estimation of Paleocurrent Direction

In clastic sediments, tilt of the plane of maximum and intermediate magnetic susceptibility commonly reflects imbrication of magnetic grains during deposition (Taira, 1989; Novak et al., 2014). The near-horizontal orientation of susceptibility maxima in all specimens is consistent with deposition of elongate mineral grains as rollers oriented perpendicular to the current direction (Tauxe, 1998; Fig. 6A). Susceptibility minima are slightly offset to the north to east-northeast from vertical, indicating a primary south to west-southwest paleocurrent direction, consistent with observations from more conventional methods (e.g., Jain et al., 1974; Cina et al., 2009; Kesari, 2010; Chirouze et al., 2012a). Similar to observations by Cina et al. (2009), paleocurrents switch from west-southwest in the lower third of Middle Siwalik samples to south-southwest in the upper two thirds of the sampled subsection (Fig. 6B).

Detrital Thermochronology

Detailed analytical results and calculated cooling ages for all new analyses are reported with 2σ errors in the GSA Data Repository (see footnote 1). Zircon fission-track analyses of river sediment samples discussed here were originally reported in Stewart et al. (2008) and Enkelmann et al. (2011).

Analyses of River Sediment Samples

White mica $^{40}Ar/^{39}Ar$ analyses from Himalayan tributaries. Detrital white mica $^{40}Ar/^{39}Ar$ analyses from three Himalayan tributary samples produce older (>10 Ma) cooling ages with narrow age ranges recording the exhumation of the specific tectono-stratigraphic units within the respective drainage area of each sample (Fig. 7). Specifically, the Yamne (sample Z) and Yang Sang (sample Y) rivers both contain a 29 Ma cooling age component that must have originated from a mica-bearing tectonic unit drained by both rivers. This source is likely a suite of crystalline metamorphic rocks (Pari Mountain formation of Singh, 1993) previously interpreted as Greater Himalayan Crystalline correlatives (Acharyya, 2007) east of the Siang River, but could alternatively be leucogranites within interpreted ophiolitic assemblages along the interpreted eastern continuation of the Indus-Yarlung suture zone (Misra, 2009). If the source is in fact crystalline metamorphic rocks east of the Siang River, then these units may have a tectonic history distinct from Greater Himalayan Crystallines west of the Siang River with which they have been correlated.

The Yang Sang River also drains Transhimalayan intrusive and metamorphic units north of the suture zone (Acharyya, 2007; Misra, 2009), which may explain the additional, smaller component of older ages around 43 Ma (see discussion in subsequent section). The Siyom River has a clearly defined 16 Ma age component sourced from Greater Himalayan Crystalline rocks within the drainage area. This age component is consistent with previous estimates of an early Miocene period of exhumation of Greater Himalayan Crystalline units along the Main Central thrust (e.g., Yin et al., 2010; Uddin et al., 2010; Mathew et al., 2013; Warren et al., 2014), exposed within the Siyom River drainage (Acharyya, 2007).

White mica $^{40}Ar/^{39}Ar$ analyses from the Siang River. White mica $^{40}Ar/^{39}Ar$ analyses of river sediment samples collected from three different locations along the main channel of the Siang River (samples A, B, and C) all have wider ranges of cooling ages than are observed in Himalayan tributaries (Fig. 7). Since we did not quantitatively determine the mineralogy of each mineral grain prior to analysis, it is possible that some age dispersion may result from the misattribution of incorrect diffusion kinetics during total fusion experiments (e.g., applying diffusion kinetics for muscovite to a phengite grain). However, we prefer to interpret cooling age variability in these samples to instead reflect the addition of mineral grains derived from new source areas in a larger drainage basin.

[1]GSA Data Repository item 2016103, thermochronologic and magnetostratigraphic sample data, and parameters for thermal model, is available at http://www.geosociety.org/pubs/ft2016.htm or by request to editing@geosociety.org.

Geological Society of America Bulletin, published online on 27 April 2016 as doi:10.1130/B31419.1

Cooling ages from Siang River samples include older ages similar to those observed in Himalayan tributaries with the addition of younger ages clustering around, and younger than, 9 Ma. We interpret these young micas in Siang River sediments to be derived from the Namche Barwa massif. This interpretation is consistent with previous interpretations of young zircon cooling ages in Siang River samples (Pik et al., 2005; Stewart et al., 2008; Enkelmann et al., 2011) and with bedrock thermochronologic data from the massif itself. Extremely young $^{40}Ar/^{39}Ar$ ages are observed in bedrock biotites from Namche Barwa (5 Ma and younger than 1 Ma; Zeitler et al., 2014); considering that white mica has a slightly higher closure temperature than biotite (McDougall and Harrison, 1999; Harrison et al., 2009), erosion of bedrock contributing the extremely young biotites could produce the slightly older (younger than 9 Ma) white mica ages we observed. Furthermore, no alternative sources of similarly young $^{40}Ar/^{39}Ar$ cooling ages have been reported within the immediate eastern syntaxial region. Biotite and K-feldspar $^{40}Ar/^{39}Ar$ cooling ages from igneous bedrock upstream of the massif are older than 8–10 Ma (e.g., Maluski et al., 1982; Coulon et al., 1986; Copeland et al., 1987, 1995; Copeland and Harrison, 1990; Harrison et al., 2000; Zeitler et al., 2014) and may be the source of the older ages observed in Siang River samples but not also observed in Himalayan tributaries.

Mica analyses producing extremely young apparent cooling ages (e.g., <4 Ma) often also exhibit a reduced percentage of radiogenic ^{40}Ar. A reduced percentage of radiogenic ^{40}Ar may result from the addition of nonradiogenic, possibly atmospheric ^{40}Ar to a truly young mica grain (McDougall and Harrison, 1999). We note, however, that no grains with apparently young (younger than 9 Ma) cooling ages also have anomalous ^{36}Ar measurements (a proxy for an atmospheric source of nonradiogenic ^{40}Ar) exceeding two standard deviations from the mean of 500–1000 mm analyses. Consequently, we do not attribute the reduced percentage of radiogenic ^{40}Ar in grains with

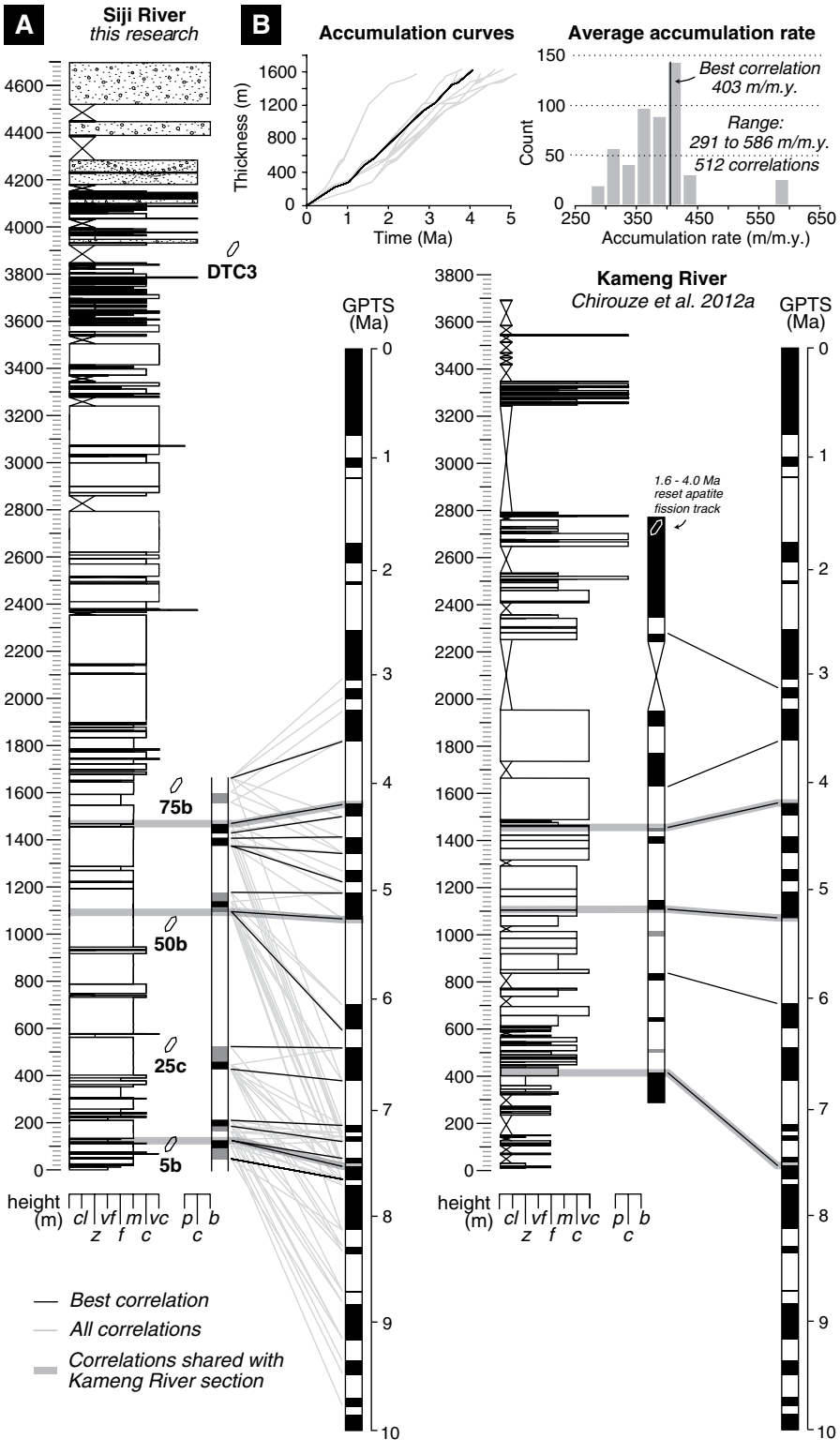

Figure 5. (A) Correlation of polarity zone sequence to the *2012 Geomagnetic Polarity Timescale* (GPTS; Gradstein et al., 2012) and comparison to a Siwalik section along the Kameng River near Bhalukpong (Chirouze et al., 2012a). We evaluated the best correlation by iterative comparison of sequence permutations to the GPTS. The best correlation minimized local variability in the accumulation rate (grain size classified as in Fig. 3). (B) Comparison of accumulation curves and accumulation rates. Our correlation shared several polarity zone–chron matches with the work of Chirouze et al. (2012a), and neither section contains evidence for a long normal polarity zone (i.e., that might correspond to the C5n.2n), indicating the entire sequence is younger than 9.9 Ma. Both sections also exhibit similar trends in grain size and bed thickness.

apparently young cooling ages to anomalous nonradiogenic ^{40}Ar contamination from an atmospheric source, and we interpret all cooling ages as thermochronologically significant. We recommend that additional step-heating experiments in future analyses might provide valuable insight to evaluate alternative mechanisms to reduce the percentages of radiogenic ^{40}Ar in Siang River minerals.

Analyses of Siwalik Samples

Coupled zircon fission-track and U-Pb analyses. By coupling new fission-track thermochronology with previously published U-Pb geochronology, we can discriminate between cooling histories from multiple source terranes. Detrital zircon U-Pb geochronology is a well-established indicator of detrital provenance in the eastern Himalaya (e.g., Stewart et al., 2008; Cina et al., 2009; Lang and Huntington, 2014). Zircons with crystallization ages younger than 300 Ma are predominantly derived from Transhimalayan intrusive units in Tibet (Zhang et al., 2012; Lang and Huntington, 2014), whereas zircons from the Namche Barwa massif are typically older than 300 Ma with the important exception of anatectic units younger than 30 Ma (Booth et al., 2004; Lang et al., 2013). To constrain exhumation of the massif specifically, we filtered fission-track analyses using the crystallization age of the same grain, only considering zircons with U-Pb ages exceeding 300 Ma, or less than 30 Ma if the U/Th ratio exceeded 10 (i.e., Th/U < 0.1), indicating a metamorphic origin (Hoskin and Schaltegger, 2003).

To interpret fission-track data, we deconvolved cooling age populations into constituent age components, or "peaks," using the DensityPlotter application of Vermeesch (2012). Overlapping analytical error on single-grain analyses reduces the interpretability of individual grain analyses, so we focus interpretation on the minimum distinguishable age component. Results including decomposed age components are presented in Figure 8 and detailed in the GSA Data Repository (see footnote 1).

The Upper Siwalik sample (DTC3) is dominated by young zircon fission-track cooling ages with two discernible age components at 1.8 and 4.1 Ma. These young ages are similar to young cooling ages previously observed in samples from the Siang River (Stewart et al., 2008; Enkelmann et al., 2011). This previously published work attributes two young cooling age components at 0.9 and 3.5 Ma observed in Siang River samples to recent exhumation of the massif, and slightly older age components at ca. 7 and ca. 11 Ma to an earlier pulse of exhumation in the late Miocene (Enkelmann et al., 2011). Similarly, we attribute the young cooling ages of sample DTC3 to a rapidly exhumed source within the Namche Barwa massif.

Middle Siwalik samples have a wider range of zircon ages, with a young age component that decreases up section. The lowest sample is dominated by Tibetan zircons, with Himalayan zircons defining only a single component

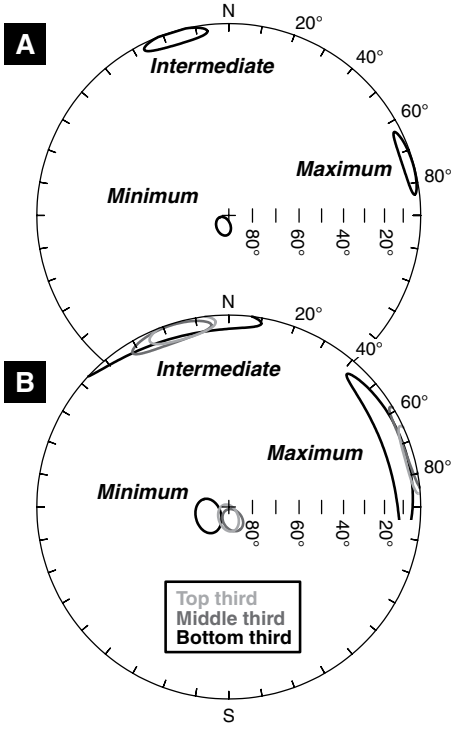

Figure 6. Lower-hemisphere projected equal-area plots of mean magnetic susceptibility orientations (corrected for bed tilt) for (A) all specimens and (B) each third of the sampled Middle Siwalik subsection. Specimens indicate a south- to west-southwest–directed paleocurrent consistent with a northern source region within the eastern Himalayan syntaxis. Ovals represent the 95% confidence region estimated from a parametric bootstrap analysis, where replacement data are perturbed by normal variation consistent with their or the population's statistical parameters (Tauxe et al., 1991; Tauxe, 1998).

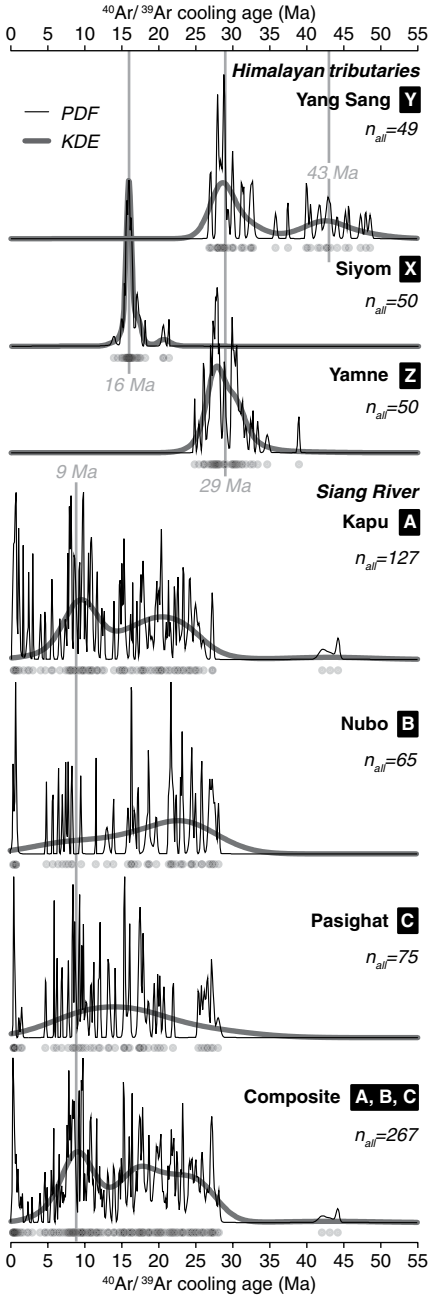

Figure 7. Detrital white mica ^{40}Ar/^{39}Ar cooling ages from modern river sediment samples (see Fig. 1 for sample locations). Cooling ages from Himalayan tributaries contain narrowly defined age populations characteristic of cooling histories for units within each drainage area. Cooling ages from three Siang River samples span a wider range that includes very young cooling ages younger than 9 Ma. The total number of single-grain analyses (n_{all}) is listed for each sample, although a few cooling ages older than 55 Ma were considered precursory to the Himalayan orogeny and were not included in data plots. Plots include area normalized, summed probability density functions (PDF, thin black lines), and kernel density estimates (KDE, thick gray lines). Kernel density estimation was determined using the DensityPlotter application of Vermeesch (2012).

Geological Society of America Bulletin, published online on 27 April 2016 as doi:10.1130/B31419.1

at 16.7 Ma. Samples 25c, 50b, and 75b are defined by three components, the youngest of which systematically decreases from 11.4 Ma to 6.0 Ma to 4.3 Ma in each sample, respectively. Older age components may originate in igneous sources in Tibet, as zircons with crystallization ages indicative of a Tibetan igneous source have relatively old (12 Ma and 26 Ma) cooling ages, or reflect an early pulse of massif exhumation preserved in older cooling ages around the massif perimeter. Previously, Enkelmann et al. (2011) attributed detrital age components older than ca. 18 Ma to either Transhimalayan or Lesser Himalayan units exposed in local Himalayan tributaries.

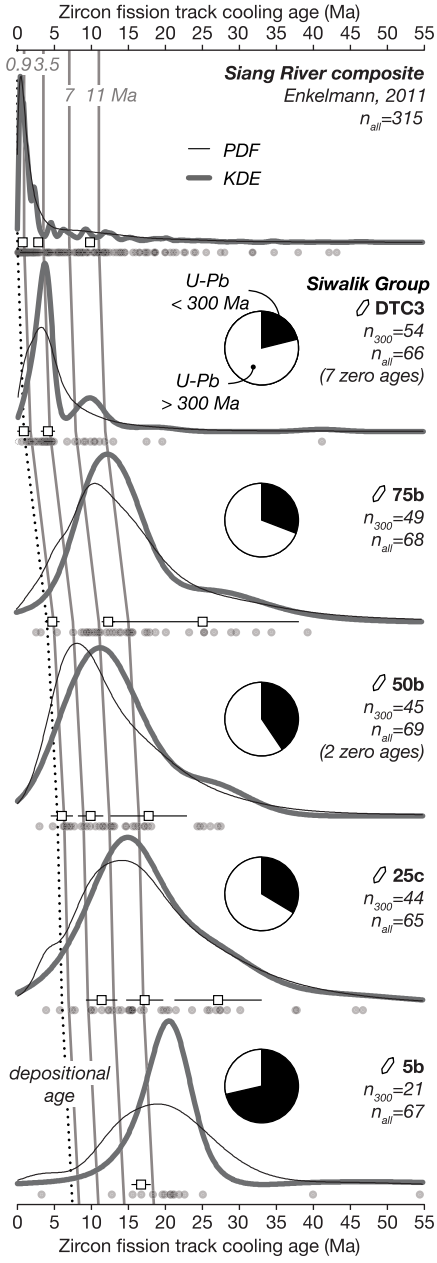

White mica $^{40}Ar/^{39}Ar$ analyses. Compared to the zircon fission-track results, $^{40}Ar/^{39}Ar$ analyses produce a wider range of cooling ages in Siwalik samples (Fig. 9). Irregular age spectra may reflect a heterogeneous distribution of the target mineral in source region bedrock (e.g., Clift et al., 2004) in addition to variability in source exhumation patterns. To avoid speculation on such complications, we restrict interpretations to the simple presence or absence of diagnostic young $^{40}Ar/^{39}Ar$ cooling ages in Siwalik samples. Whereas interpretations of detrital fission-track data rely on age component decomposition to identify the youngest representative age signal, individual white mica grain ages can be interpreted with greater confidence due to the high analytical precision of $^{40}Ar/^{39}Ar$ analyses.

Analysis of the Upper Siwalik sample DTC3 primarily produced older cooling ages matching observations from Himalayan tributaries, with the small addition of grains younger than 4 Ma originating from the Namche Barwa massif. The predominance of older Himalayan cooling ages in the Upper Siwalik may reflect recycling of older ages from Himalayan tectono-stratigraphic units in a depositional area closer to the mountain front but removed from the axial basin depocenter. Grains younger than 4 Ma observed in this sample may have been eroded from recently exhumed rocks of the massif or recycled from upper portions of the Middle Siwalik. Whereas the modern Siang River sample contained a significant component of very young ages with a reduced percentage of radiogenic argon, only a few cooling ages with similarly reduced percentage of radiogenic argon were observed in sample DTC3, and none were observed in samples from lower stratigraphic samples.

The youngest single grain cooling ages in Middle Siwalik samples systematically decreased up section. The lowest sample, 5b, was dominated by older ages between 20 and 35 Ma. Such ages were also observed in Himalayan tributaries draining portions of the suture zone, suggesting that this lowest sample may record early erosion of the suture zone prior to deep exhumation of the Namche Barwa massif. This interpretation may be further supported by a dearth of zircons with characteristic Himalayan crystallization ages in this sample. The youngest individual ages from the remaining Middle Siwalik samples decreased from 12.9 Ma to 8.1 Ma to 6.9 Ma up section for samples 25c, 50b, and 75b, respectively. The upward younging of minimum ages may reflect sustained, and potentially accelerating exhumation of the Namche Barwa massif.

Figure 8. Detrital zircon fission-track cooling ages from Upper and Middle Siwalik samples compared to ages from modern Siang River samples (Enkelmann et al., 2011). U-Pb dating of the same Upper and Middle Siwalik zircons permits differentiation of cooling ages by source region. Pie charts indicate the percentages of Himalayan zircons with crystallization ages older than 300 Ma and Transhimalayan zircons younger than 300 Ma. Only Himalayan zircons are illustrated in line plots. Young cooling age components attributed to the Namche Barwa massif (Enkelmann et al., 2011) persist in young lag times of Upper and Middle Siwalik samples until 25c and 5b. Sample 5b is dominated by zircons with a Transhimalayan U-Pb age provenance, which may reflect erosion of the suture zone and Transhimalaya intrusive units prior to exhumation of the Namche Barwa massif. Fission-track age components (white boxes) were determined with the DensityPlotter application of Vermeesch (2012). The total number of analyses (n_{all}) and number of zircons with U-Pb ages older than 300 Ma (n_{300}) are reported. Plots include area normalized, summed probability density functions (PDF, thin black lines) , and kernel density estimates (KDE, thick gray lines).

DISCUSSION

Interpretation of Thermochronological Lag Time

We interpret the exhumation history of the source rocks contributing detritus to the Himalayan foreland based on calculation of detrital thermochronological lag time (Bernet and Garver, 2005). Thermochronological lag time is the difference between a minimum detrital mineral cooling age (or age component) and the depositional age of the sampled sedimentary horizon (Garver and Brandon, 1994). When the residence time of intermontane sediment storage is small relative to the time scale of mineral cooling (e.g., Garver et al., 1999; Bernet et al., 2004), and dynamic perturbations to the subsurface thermal field may be accounted for with thermal modeling (e.g., Braun et al., 2006), lag time is indicative of source region paleo-exhumation rates. Systematic variation in lag time with depositional age may elucidate fundamental changes in the exhumation of source terranes. For example, an up-section lag time decrease (i.e., a decrease in lag time with decreasing depositional age) may indicate acceleration of source rock exhumation during a constructive phase of orogenesis (Bernet and

Garver, 2005). Constant lag time may indicate constant or steady-state exhumation (e.g., Willett and Brandon, 2002; Burbank et al., 2007).

We calculated thermochronologic lag time for minimum single-grain $^{40}Ar/^{39}Ar$ cooling ages and minimum fission-track age components in Siwalik samples (Fig. 10). In both data sets, lag time decreases up section, approaching cooling ages observed in modern river sediment samples (i.e., younger than 2 Ma fission track ages—Stewart et al., 2008; Enkelmann et al., 2011; younger than 4 Ma $^{40}Ar/^{39}Ar$ ages) by the stratigraphic horizon at sample 50b, magnetostratigraphically correlated between 5 and 6 Ma. After this stratigraphic horizon, lag times remain consistently low. We interpret the lag time pattern prior to sample 50b to result from an increase in source region exhumation rates in the late Miocene, and the pattern after sample 50b to indicate rapid exhumation sustained since ca. 5 Ma. Because lag time decreases to within the range of modern bedrock cooling ages uniquely attributed to the Namche Barwa massif, and no alternative sources of similarly rapid exhumation have been reported within the syntaxial region, we attribute this exhumation rate increase specifically to unroofing of the Namche Barwa massif.

Thermal Modeling

To quantitatively constrain the timing and magnitude of an exhumation rate change in the source region, we used a simplified version of Pecube, a finite-element numerical code often used for predicting thermochronological data (Fig. 11A; Braun, 2003; Braun et al., 2012) to predict a time series of cooling ages resulting from a step change in the late Miocene exhumation rate. Pecube accounts for heat advection in mineral cooling—an important influence in regions of such extreme rock exhumation rates (Braun et al., 2006). Our simple model assumes only vertical rock exhumation since both the crustal-scale folding (Burg et al., 1998) and pop-up structures (Ding et al., 2001) proposed as exhumation mechanisms for the Namche Barwa massif are dominated by vertical rock uplift. Similar to prior modeling by Zeitler et al. (2014) of the area surrounding Namche Barwa, our approach does not account for the potential effects of lateral heat transfer, which are assumed to be insignificant relative to the extreme vertical component of heat transport. Our model further neglects the influence of changing topographic relief, which is not independently well constrained, as previous modeling of detrital cooling populations indicates that even large changes in topographic relief have only a secondary effect on the range of a detrital age distribution (Whipp et al., 2009) and do not significantly influence median ages (Ruhl and Hodges, 2005). Thermal parameters used in the model are comparable to previous thermal models of the eastern Himalaya (e.g., Robert et al., 2011; Adlakha et al., 2013) and are detailed in the GSA Data Repository (see footnote 1).

Our simple approach predicts cooling ages from scenarios reflecting changes in three parameters: the time of a change in exhumation rate (between 1 and 15 Ma), a factor increase in the exhumation rate (1–20 fold), and the final exhumation rate, which was fixed between 5 km/m.y. and 10 km/m.y., characteristic of rates interpreted from bedrock samples. For each model run, we used the root mean squared error to separately compare cooling age predictions to our observations for each thermochronometer system. The composite root mean squared

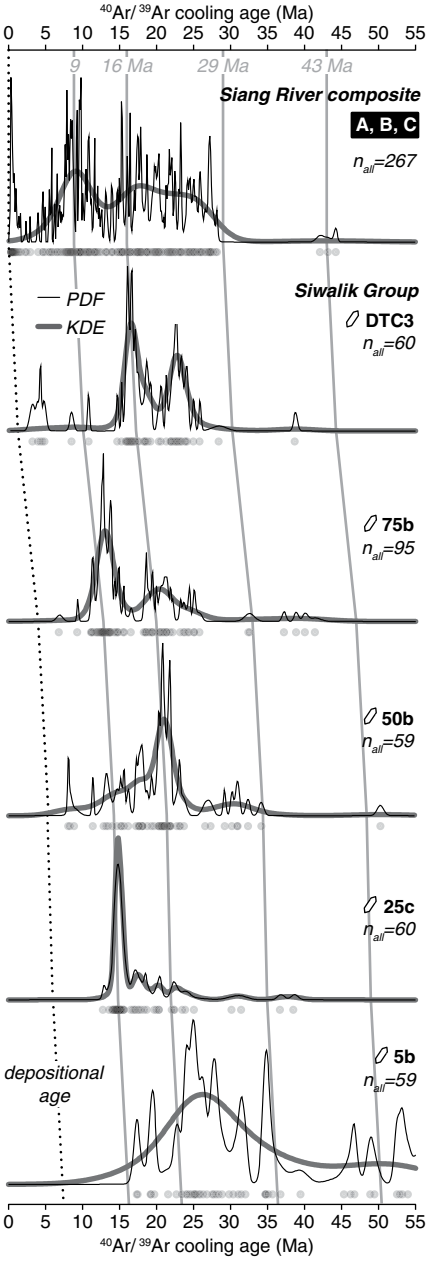

Figure 9. Detrital white mica $^{40}Ar/^{39}Ar$ cooling ages from Upper and Middle Siwalik samples compared to modern samples from the Siang River and characteristic age ranges from Himalayan tributaries. We interpret the predominance of Himalayan ages in the Upper Siwalik sample to reflect Siwalik recycling and increased contribution from local Himalayan sources. Detrital samples contain young cooling ages relative to depositional age (young lag times) that disappear in lower samples 25c and 5b. The lowest sample, 5b, contains much older ages similar to those observed in tributaries draining Himalayan crystalline and suture zone units, possibly supporting the interpretation from fission-track ages that this sample reflects contribution from the suture zone and Transhimalayan intrusive units prior to massif exhumation. The total number of single-grain analyses (n_{all}) is listed for each sample. Plots include area normalized, summed probability density functions (PDF, thin black lines), and kernel density estimates (KDE, thick gray lines).

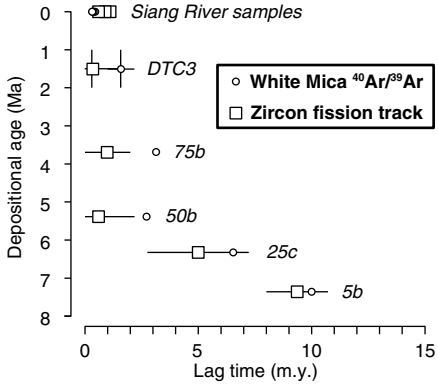

Figure 10. Thermochronologic lag time systematically decreases to within the range of cooling ages from the Siang River by ca. 5 Ma. Lag time was calculated from youngest fission-track age components (white squares) and minimum $^{40}Ar/^{39}Ar$ single-grain ages (white circles) from Siang River samples. Siang River fission-track age components are from Enkelmann et al. (2011).

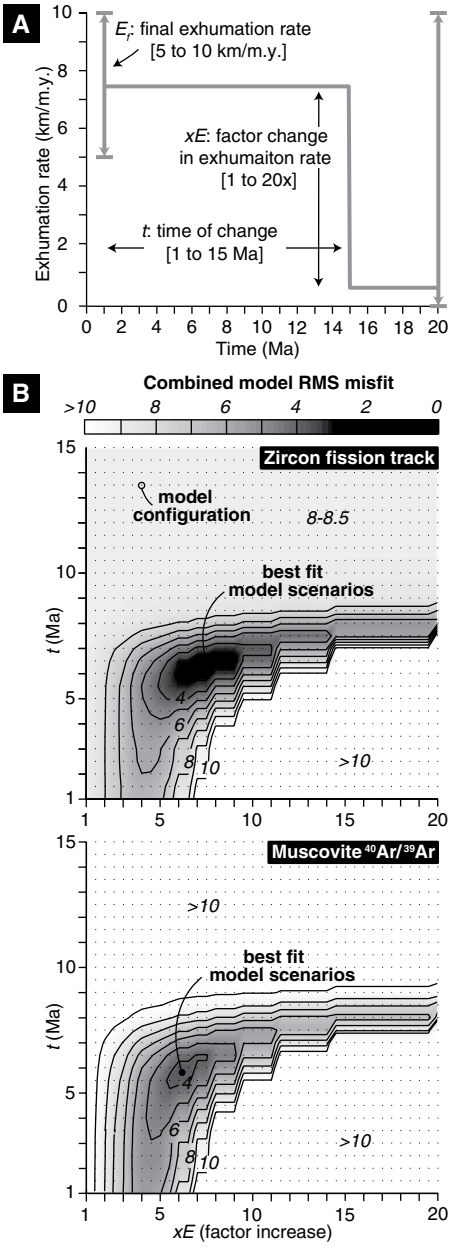

Figure 11. Results of thermal modeling used to predict thermochronologic lag time. (A) We varied the factor change (*xE*) and timing (*t*) of a step-wise increase in exhumation rate, keeping the final exhumation rate (E_f) fixed between 5 and 10 km/m.y. to stay consistent with observations from bedrock data. (B) Contoured plots of root-mean-squared (RMS) misfit between predicted and observed lag times. Both thermochronologic data sets are best explained by a 5–10-fold increase in exhumation rate between 5 and 7 Ma. Each gridded point represents an individual model scenario. RMS misfit is summed over six sets of model output where the final exhumation rate (E_f) varied between 5 and 10 km/m.y.

error from all six sets of models is shown in Figure 11B.

While this modeling remains simple, it consistently indicates that the observed change in lag time is best explained by a 5–10-fold increase in the source region exhumation rate between 5 and 7 Ma. However, lacking additional observations from lowest Middle Siwalik or Lower Siwalik units older than 8 Ma, the maximum bound on the onset of rapid exhumation is not well constrained. Thermal modeling of bedrock cooling ages surrounding the Namche Barwa massif by Zeitler et al. (2014) instead indicates that rapid exhumation initiated at 10 Ma, and we anticipate that further analyses of Lower Siwalik samples may constrain a lower bound on this onset time more precisely.

Emergence of Thermo-Mechanical Feedbacks

Our interpretation of extreme exhumation rates sustained since 5 Ma may reflect the emergence of the thermo-mechanical feedbacks proposed by Zeitler et al. (2001). Zeitler et al. (2001) originally proposed that thermo-mechanical feedbacks may have emerged in both Himalayan syntaxes following the capture of large, longitudinal river systems—specifically, capture of the Yarlung River in the eastern syntaxis by a Brahmaputra River tributary. Since observations of Tibetan detritus in foreland basin units (Cina et al., 2009; Lang and Huntington, 2014) and distal Bengal fan deposits (Bracciali et al., 2015) indicate that if such a capture event occurred, it must have predated deposition of these units in the middle or early Miocene, we consider that such a discrete erosional event is unlikely to have directly resulted in increased rock exhumation rates after 5 Ma. Instead, increased exhumation rates between 5 and 7 Ma, or even 10 Ma, may represent a period of incision into the southeastern margin of the Tibetan Plateau as the ancestral Yarlung River system adjusted to increased rock uplift while maintaining a low-elevation base level.

Recent documentation of >550 m of sediment aggradation along the Yarlung River upstream of the Tsangpo Gorge suggests that an ancestral Yarlung River system may have previously achieved a graded or near-graded longitudinal profile (Wang et al., 2014). Cosmogenic dating of buried sediment collected from a core ~150 km upstream of the gorge provided a ca. 2–2.5 Ma minimum constraint on the timing of Yarlung aggradation, which Zeitler et al. (2015) extrapolated to 3–4 Ma based on the maximum estimated sedimentary thickness closer to the gorge. If increased rock uplift at the margin of the Tibetan Plateau steepened the ancestral river profile beginning in the late Miocene, then reduction of the river's gradient above the newly development knick zone, a climatic reduction of river transport capacity, or both may explain aggradation in the Pliocene. Since 5 Ma, thermo-mechanical feedbacks may have sustained rapid exhumation in a steep knick zone at the plateau margin.

Lag Time Across the Himalaya

Geodynamic modeling of subduction in generalized syntaxial regions predicts locally elevated rock uplift as a consequence of a curved subducting plate geometry (Bendick and Ehlers, 2014). If a similar subducting plate geometry characterizes the eastern margin of the Himalayan orogen, enhanced rock uplift rates may have developed from stiffening of the subducting Indian crust. In response, thermo-mechanical feedbacks may have only developed where a large, antecedent river system crossing the syntaxis could sustain sufficiently high rates of crustal exhumation (Koons et al., 2013). To determine how our observations compare to transverse river drainages outside of syntaxial regions, we compared lag time data across the Himalayan orogen.

We compiled lag time data from eight locations across the orogen, including lag time calculated from minimum zircon fission-track age components and minimum single-grain white mica $^{40}Ar/^{39}Ar$ analyses from six locations along the Himalayan front and both Himalayan syntaxes (Fig. 12A). To illustrate the general trend of lag time with depositional age, we fit linear regressions to each data set independently (Fig. 12B), and we observe that decreasing thermochronologic lag time up stratigraphic section is only observed in foreland sequences proximal to the Himalayan syntaxes.

Along the Himalayan front, lag times calculated from minimum zircon fission-track age components have remained constant or increased since the middle Miocene. This trend has been previously interpreted to reflect constant Himalayan exhumation rates of ~1–2 km/m.y. across the central and eastern Himalaya since ca. 16–13 Ma (Bernet et al., 2006; Chirouze et al., 2013) or possibly reduced Miocene exhumation in eastern Nepal (Chirouze et al., 2012b). Lag times calculated from minimum single-grain white mica $^{40}Ar/^{39}Ar$ ages have increased since the Early Miocene, and this is interpreted to represent a decrease in Greater Himalayan exhumation as thrusting propagated forward to Lower Himalayan sequences (White et al., 2002; Szulc et al., 2006; Najman et al., 2009).

In contrast, lag times reported from the western Himalayan syntaxis have decreased since

the early Miocene. Lag times calculated from minimum zircon fission-track age components and single-grain white mica $^{40}Ar/^{39}Ar$ ages have been interpreted to represent a progressive increase in source exhumation rate since ca. 18 Ma (Cerveny et al., 1988; see decomposition from Ruiz and Seward, 2006; Najman et al., 2003; Chirouze et al., 2015), broadly consistent with the observations reported here for the eastern Himalayan syntaxis. If this emergence of very young lag times indicates the onset of thermo-mechanical feedbacks, then this observation suggests that syntaxial regions may be the only locations where thermo-mechanical feedbacks have developed in the Himalayan orogen, and potentially much earlier in the western syntaxis than the eastern syntaxis. New analyses from additional locations and lower stratigraphic levels will be useful to further compare exhumation histories across the Himalaya.

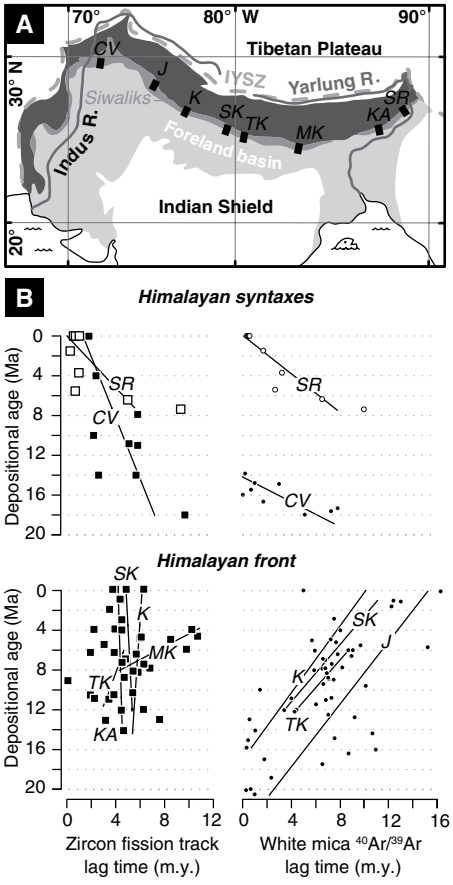

Figure 12. Compilation of lag time data from Siwalik Group across the Himalaya. (A) Locations of sections illustrated on a simplified map of tectonic and foreland basin units (CV—Chinji village area, J—Jogindernagar area, K—Karnali River, SK—Surai Khola, TK—Tinau Khola, MK—Muksar Khola, KA—Kameng River, SR—Siji River; modified from Critelli and Garzanti, 1994). (B) Linear regressions of lag time from Siwalik sections proximal to the Himalayan syntaxes indicate an up-section lag time decrease in both thermochronologic systems. In contrast, regressions of lag time data from sections along the Himalayan front indicate an increase or constant lag time up section. Lag time is calculated from minimum zircon fission-track age components and minimum $^{40}Ar/^{39}Ar$ white mica single-grain ages. See text for data references.

SUMMARY AND CONCLUSIONS

The Himalayan syntaxes host exceptional landscapes where efficient erosional systems have rapidly exhumed young metamorphic massifs at the eastern and western margins of the orogen. This study extends the record of crustal exhumation preserved in bedrock thermochronological cooling ages of the eastern Himalayan syntaxis by reconstructing the exhumation history from detrital cooling ages in foreland basin units. We focused on a proximal 4.6-km-thick stratigraphic section for which sedimentary provenance had been studied previously using detrital zircon U-Pb geochronology. Detailed stratigraphic surveys, magnetostratigraphy, detrital white mica $^{40}Ar/^{39}Ar$ thermochronology, and fission-track dating of detrital zircons for which previous U-Pb ages were available enabled us to measure thermochronologic lag time since the late Miocene.

Lag times for both thermochronometers decrease up section in the Middle Siwalik, best explained by a 5–10-fold increase in syntaxial exhumation rate between 7 and 5 Ma. Since 5 Ma, extremely rapid exhumation rates have been sustained in the Namche Barwa region, an observation that may be consistent with the development of thermo-mechanical feedbacks in the eastern Himalayan syntaxis, and which suggests that the steep topographic gradients and rapid surface erosion presently exhuming the massif may be long-lived features of this landscape. Because a late Miocene increase in rapid exhumation significantly postdates a hypothesized river capture event in the early or middle Miocene, we conclude that integration of the river system did not initiate rapid exhumation of the Namche Barwa massif. Instead, we suggest that exhumation rates increased in the late Miocene as an antecedent river system adjusted to tectonic uplift of its headwaters while maintaining a low-elevation base level.

Similar observations of accelerating rock exhumation are observed in lag time studies of Siwalik units proximal to the western Himalayan syntaxis, but not also in studies from across the main Himalayan front. Considering our observations within the context of this broader pattern, we emphasize the importance of antecedent river drainage in the development of localized thermo-mechanical feedbacks that may have sustained steep topography, rapid exhumation, and high sedimentary discharges at the Himalayan syntaxes for a considerable expanse of time.

ACKNOWLEDGMENTS

We acknowledge funding from the National Science foundation (EAR 0955309 and EAR 1349279 to Huntington), the Geological Society of America (Graduate Student Research Grant to Lang), and the Quaternary Research Center at the University of Washington. We thank M. Turzewski, G. Messe, K. Bage, and O. Tayeng for field assistance; J. Wartho, K. Atakturk, K. Sumner, and B. Novak for laboratory assistance; and A. Cavosie and A. Yin for editorial support. This paper greatly benefited from detailed reviews from Y. Najman and P. Zeitler, as well as discussion with D. Montgomery, B. Hallet, T. Ehlers, and B. Adams.

REFERENCES CITED

Acharyya, S.K., 2007, Evolution of the Himalayan Paleogene foreland basin, influence of its litho-packet on the formation of thrust-related domes and windows in the eastern Himalayas—A review: Journal of the Geological Society of India, v. 31, p. 1–17.

Adlakha, V., Lang, K.A., Patel, R.C., Lal, N., and Huntington, K.W., 2013, Rapid long-term erosion in the rain shadow of the Shillong Plateau, eastern Himalaya: Tectonophysics, v. 582, p. 76–83, doi:10.1016/j.tecto.2012.09.022.

Agarwal, R.P., Srivastava, A.K., and Maithani, A., 1991, Geology of the eastern Himalayan Foothill Belt of Bhutan and Arunachal Pradesh: An overview: Journal of Himalayan Geology, v. 2, no. 2, p. 197–205.

Ali, J.R., Aitchison, J.C., Chik, S.Y.S., Baxter, A.T., and Bryan, S.E., 2012, Paleomagnetic data support Early Permian age for the Abor volcanics in the lower Siang Valley, NE India: Significance for Gondwana-related break-up models: Journal of Asian Earth Sciences, v. 50, p. 105–115, doi:10.1016/j.jseaes.2012.01.007.

Armijo, R., Tapponnier, P., and Han, T., 1989, Late Cenozoic right-lateral strike-slip faulting in southern Tibet: Journal of Geophysical Research, v. 94, p. 2787–2838, doi:10.1029/JB094iB03p02787.

Avdeev, B., Niemi, N.A., and Clark, M.K., 2011, Doing more with less: Bayesian estimation of erosion models with detrital thermochronometric data: Earth and Planetary Science Letters, v. 305, no. 3–4, p. 385–395, doi:10.1016/j.epsl.2011.03.020.

Baruah, J.M.B., Handique, G.K., Rath, S., and Mallick, R.K., 1992, Exploration for Palaeocene–Lower Eocene hydrocarbon prospects in the eastern parts of Upper Assam basin: Indian Journal of Petroleum Geology, v. 1, p. 117–129.

Baruah, P.K., 2001, Sandstone composition and tectonoprovenance of Dafla and Subansiri formations from Kimin-Zero road section of Arunachal Pradesh: Himalayan Geology, v. 22, p. 41–54.

Beaumont, C., 1981, Foreland basins: Geophysical Journal of the Royal Astronomical Society, v. 65, p. 291–329, doi:10.1111/j.1365-246X.1981.tb02715.x.

Beaumont, C., Fullsack, P., and Hamilton, J., 1992, Erosional control of active compressional orogens, *in* McClay, K.R., ed., Thrust Tectonics: London, Chapman and Hall, p. 1–18, doi:10.1007/978-94-011-3066-0_1.

Beaumont, C., Kooi, H., and Willet, S., 2000, Coupled tectonic-surface process models with applications

to rifted margins and collisional orogens, *in* Summerfield, M.A., ed., Geomorphology and Global Tectonics: Chichester, UK, John Wiley and Sons, p. 29–55.

Bendick, R., and Ehlers, T., 2014, Extreme localized exhumation at syntaxes initiated by subduction geometry: Geophysical Research Letters, v. 41, no. 16, p. 5861–5867, doi:10.1002/2014GL061026.

Benvenuti, M., and Martini, I.P., 2002, Analysis of terrestrial hyperconcentrated flows and their deposits, *in* Baker, V., Martini, I.P., and Garzon, G., eds., Floods and Megaflood Processes and Deposits: International Association of Sedimentologists Special Publication 32, p. 167–193, doi:10.1002/9781444304299.ch10.

Bernet, M., and Garver, J.I., 2005, Fission-track analysis of detrital zircon, *in* Reiners, P.W., and Ehlers, T.A., eds., Low-Temperature Thermochronology: Techniques, Interpretations and Applications: Reviews in Mineralogy and Geochemistry, v. 58, p. 205–238.

Bernet, M., Brandon, M.T., Garver, J.I., and Molitor, B.R., 2004, Fundamentals of detrital zircon fission-track analysis for provenance and exhumation studies with examples from the European Alps, *in* Bernet, M., and Spiegel, C., eds., Detrital Thermochronology—Provenance Analysis, Exhumation, and Landscape Evolution of Mountain Belts: Geological Society of America Special Paper 378, p. 25–36.

Bernet, M., van der Beek, P., Pik, R., Huyghe, P., Mugnier, J.-L., Labrin, E., and Szulc, A., 2006, Miocene to Recent exhumation of the central Himalaya determined from combined detrital zircon fission-track and U/Pb analysis of Siwalik sediments, western Nepal: Basin Research, v. 18, p. 393–412, doi:10.1111/j.1365-2117.2006.00303.x.

Bhareli, B., and Ratnam, C., 1978, Some contributions to the geology of northeastern India: Himalayan Geology, v. 8, no. 2, p. 757–768.

Booth, A.L., Zeitler, P.K., Kidd, W.S.F., Wooden, J., Liu, Y., Idleman, B., Hren, M., and Chamberlain, C.P., 2004, U-Pb zircon constraints on the tectonic evolution of southeastern Tibet, Namche Barwa area: American Journal of Science, v. 304, no. 10, p. 889–929, doi:10.2475/ajs.304.10.889.

Booth, A.L., Chamberlain, C.P., Kidd, W.S.F., and Zeitler, P.K., 2009, Constraints on the metamorphic evolution of the eastern Himalayan syntaxis from geochronologic and petrologic studies of Namche Barwa: Geological Society of America Bulletin, v. 121, p. 385–407, doi:10.1130/B26041.1.

Bracciali, L., Najman, Y., Parrish, R.R., Akhter, S.H., and Millar, I., 2015, The Brahmaputra tale of tectonics and erosion: Early Miocene river capture in the eastern Himalaya: Earth and Planetary Science Letters, v. 415, p. 25–37, doi:10.1016/j.epsl.2015.01.022.

Brandon, M.T., and Vance, J.A., 1992, Tectonic evolution of the Cenozoic Olympic subduction complex, Washington State, as deduced from fission-track ages for detrital zircons: American Journal of Science, v. 292, p. 565–636, doi:10.2475/ajs.292.8.565.

Braun, J., 2003, Pecube: A finite-element code to solve the 3D heat transport equation including the effects of a time-varying, finite amplitude surface topography: Computers & Geosciences, v. 29, p. 787–794, doi:10.1016/S0098-3004(03)00052-9.

Braun, J., van der Beek, P., and Batt, G., 2006, Quantitative Thermochronology: Cambridge, UK, Cambridge University Press, 270 p., doi:10.1017/CBO9780511616433.

Braun, J., van der Beek, P., Valla, P., Robert, X., Herman, F., Glotzbach, C., Pedersen, V., Perry, C., Simon-Labric, T., and Prigent, C., 2012, Quantifying rates of landscape evolution and tectonic processes by thermochronology and numerical modeling of crustal heat transport using PECUBE: Tectonophysics, v. 524–525, p. 1–28, doi:10.1016/j.tecto.2011.12.035.

Bristow, C.S., and Best, J.L., 1993, Braided rivers: Perspectives and problems, *in* Best, J.L. and Bristow, C.S., eds., Braided Rivers: Geological Society of London Special Publication 75, p. 1–11, doi:10.1144/GSL.SP.1993.075.01.01.

Brookfield, M.E., 1998, The evolution of the great river systems of southern Asia during the Cenozoic India-Asia collision: Rivers draining southwards: Geomorphology, v. 22, no. 3–4, p. 285–312, doi:10.1016/S0169-555X(97)00082-2.

Burbank, D.W., 1992, Causes of recent Himalayan uplift deduced from deposited patterns in the Ganges basin: Nature, v. 357, p. 680–683, doi:10.1038/357680a0.

Burbank, D.W., Leland, J., Fielding, E., Anderson, R.S., Brozovic, N., Reid, M.R., and Duncan, C., 1996, Bedrock incision, rock uplift and threshold hillslopes in the northwestern Himalayas: Nature, v. 379, p. 505–510, doi:10.1038/379505a0.

Burbank, D.W., Brewer, I.D., Sobel, E.R., and Bullen, M.E., 2007, Single-crystal dating and the detrital record of orogenesis, *in* Nichols, G., Williams, E., and Paola, C., eds., Sedimentary Processes, Environments and Basins: A Tribute to Peter Friend: Malden, Massachusetts, Blackwell Publishing, p. 253–281, doi:10.1002/9781444304411.ch12.

Burg, J.P., and Podladchikov, Y., 2000, From buckling to asymmetric folding of the continental lithosphere: Numerical modeling and application to the Himalayan syntaxes, *in* Khan, M.A., Treloar, P.J., Searle, M.P., and Jan, M.Q., eds., Tectonics of the Nanga Parbat Syntaxis and the Western Himalaya: Geological Society of London Special Publication 170, p. 219–236, doi:10.1144/GSL.SP.2000.170.01.12.

Burg, J.P., and Schmalholz, S.M., 2008, Viscous heating allows thrusting to overcome crustal-scale buckling: Numerical investigation with application to the Himalayan syntaxes: Earth and Planetary Science Letters, v. 274, p. 189–203, doi:10.1016/j.epsl.2008.07.022.

Burg, J.-P., Nievergelt, P., Oberli, F., Seward, D., Davy, P., Mauring, J.-C., Diao, Z., and Meier, M., 1998, The Namche Barwa syntaxis: Evidence for exhumation related to compressional crustal folding: Journal of Asian Earth Sciences, v. 16, p. 239–252, doi:10.1016/S0743-9547(98)00002-6.

Burgess, W.P., Yin, A., Dubey, C.S., Shen, Z.K., and Kelty, T.K., 2012, Holocene shortening across the Main Frontal thrust zone in the eastern Himalaya: Earth and Planetary Science Letters, v. 357–358, p. 152–167, doi:10.1016/j.epsl.2012.09.040.

Cerveny, P.F., Naeser, N.D., Zeitler, P.K., Naeser, C.W., and Johnson, N.M., 1988, History of uplift and relief of the Himalaya during the past 18 million years: Evidence from fission-track ages of detrital zircons from sandstones of the Siwalik Group, *in* Kleinspehn, K.L., and Paola, C., eds., New Perspectives in Basin Analysis: New York, Springer, p. 43–61, doi:10.1007/978-1-4612-3788-4_3.

Chew, D.M., and Donelick, R.A., 2012, Combined apatite fission-track and U-Pb dating by LA-ICP-MS and its application in apatite provenance analysis, *in* Sylvester, P., ed., Quantitative Mineralogy and Microanalysis of Sediments and Sedimentary Rocks: St. John's, Newfoundland and Labrador, Mineralogical Association of Canada, Short Course 42, p. 219–247.

Chirouze, F., Dupont-Nivet, G., Huyghe, P., van der Beek, P., Chakraborti, T., Bernet, M., and Erens, V., 2012a, Magnetostratigraphy of the Neogene Siwalik Group of far eastern Himalaya, Kameng section, Arunachal Pradesh, India: Journal of Asian Earth Sciences, v. 44, p. 117–135, doi:10.1016/j.jseaes.2011.05.016.

Chirouze, F., Bernet, M., Huyghe, P., Erens, V., Dupont-Nivet, G., and Senebier, F., 2012b, Detrital thermochronology and sediment petrology of the Middle Siwaliks along the Muksar Khola section in eastern Nepal: Journal of Asian Earth Sciences, v. 44, p. 94–106, doi:10.1016/j.jseaes.2011.01.009.

Chirouze, F., Huyghe, P., van der Beek, P., Chauvel, C., Chakraborty, T., Dupont-Nivet, G., and Bernet, M., 2013, Tectonics, exhumation and drainage evolution of the eastern Himalaya since 13 Ma from detrital geochemistry and thermochronology, Kameng River section, Arunachal Pradesh: Geologic Society of America Bulletin, v. 125, p. 523–538.

Chirouze, F., Huyghe, P., Chauvel, C., van der Beek, P., Bernet, M., and Mugnier, J.-L., 2015, Stable drainage pattern and variable exhumation in the Western Himalaya since the middle Miocene: The Journal of Geology, v. 123, no. 1, p. 1–20, doi:10.1086/679305.

Cina, S.E., Yin, A., Grove, M., Dubey, C.S., Shukla, D.P., Lovera, O.M., Kelty, T.K., Gehrels, G.E., and Foster, D.A., 2009, Gangdese arc detritus within the eastern Himalayan Neogene foreland basin: Implications for the Neogene evolution of the Yalu-Brahmaputra River system: Earth and Planetary Science Letters, v. 285, p. 150–162, doi:10.1016/j.epsl.2009.06.005.

Clark, M.K., Schoenbohm, L.M., Royden, L.H., Whipple, K.X., Burchfiel, B.C., Zhang, X., Tang, W., Wang, E., and Chen, L., 2004, Surface uplift, tectonics and erosion of eastern Tibet from large-scale drainage patterns: Tectonics, v. 23, p. 20, doi:10.1029/2002TC001402.

Clift, P.D., Campbell, I.H., Pringle, M.S., Carter, A., Zhang, X., Hodges, K.V., Khan, A.A., and Allen, C.M., 2004, Thermochronology of the modern Indus River bedload: New insight into the controls on the marine stratigraphic record: Tectonics, v. 23, p. 17, doi:10.1029/2003TC001559.

Copeland, P., and Harrison, T.M., 1990, Episodic rapid uplift in the Himalaya revealed by $^{40}Ar/^{39}Ar$ analysis of detrital K-feldspar and muscovite, Bengal Fan: Geology, v. 18, p. 354–357, doi:10.1130/0091-7613(1990)018<0354:ERUITH>2.3.CO;2.

Copeland, P., Harrison, T.M., Kidd, W.S.F., Ronghua, X., and Yuquan, Z., 1987, Rapid early Miocene acceleration of uplift in the Gangdese Belt, Xizang (southern Tibet), and its bearing on accommodation mechanisms of the India-Asia collision: Earth and Planetary Science Letters, v. 86, no. 2–4, p. 240–252, doi:10.1016/0012-821X(87)90224-X.

Copeland, P., Harrison, T.M., Yun, P., Kidd, W.S.F., Roden, M., and Yuquan, Z., 1995, Thermal evolution of the Gangdese batholith, southern Tibet: A history of episodic unroofing: Tectonics, v. 14, p. 223–236, doi:10.1029/94TC01676.

Coulon, C., Maluski, H., Bollinger, C., and Wang, S., 1986, Mesozoic and Cenozoic volcanic rocks from central and southern Tibet: $^{39}Ar/^{40}Ar$ dating, petrological characteristics and geodynamical significance: Earth and Planetary Science Letters, v. 79, p. 281–302, doi:10.1016/0012-821X(86)90186-X.

Craw, D., Koons, P.O., Zeitler, P.K., and Kidd, W.S.F., 2005, Fluid evolution and thermal structure in the rapidly exhuming gneiss complex of Namche Barwa–Gyala Peri, eastern Himalayan syntaxis: Journal of Metamorphic Geology, v. 23, no. 9, p. 829–845.

Critelli, S., and Garzanti, E., 1994, Provenance of the Lower Tertiary Murree redbeds (Hazara-Kashmir syntaxis, Pakistan) and initial rising of the Himalayas: Sedimentary Geology, v. 89, p. 265–284, doi:10.1016/0037-0738(94)90097-3.

Davis, D., Suppe, J., and Dahlen, F.A., 1983, Mechanics of fold-and-thrust belts and accretionary wedges: Journal of Geophysical Research, v. 88, p. 1153–1172, doi:10.1029/JB088iB02p01153.

DeCelles, P.G., Gehrels, G.E., Quade, J., Ojha, T.P., Kapp, P.A., and Upreti, B.N., 1998, Neogene foreland basin deposits, erosional unroofing, and the kinematic history of the Himalayan fold-thrust belt, western Nepal: Geological Society of America Bulletin, v. 110, p. 2–21, doi:10.1130/0016-7606(1998)110<0002:NFBDEU>2.3.CO;2.

Ding, L., Zhong, D., Yin, A., Kapp, P., and Harrison, T.M., 2001, Cenozoic structural and metamorphic evolution of the eastern Himalayan syntaxis (Namche Barwa): Earth and Planetary Science Letters, v. 192, p. 423–438, doi:10.1016/S0012-821X(01)00463-0.

Dodson, M.H., 1973, Closure temperature in cooling geochronological and petrological systems: Contributions to Mineralogy and Petrology, v. 40, p. 259–274, doi:10.1007/BF00373790.

Donelick, R.A., O'Sullivan, P.B., and Ketcham, R.A., 2005, Apatite fission-track analysis, *in* Reiners, P.W., and Ehlers, T.A., eds., Low-Temperature Thermochronology: Techniques, Interpretations and Applications: Reviews in Mineralogy and Geochemistry, v. 58, p. 49–94.

Dutta, S.K., 1980, Palynostratigraphy of the sedimentary formations of Arunachal Pradesh—2. Palynology of the Siwalik equivalent rocks of Kameng District: Geophytology, v. 10, p. 5–13.

Enkelmann, E., Ehlers, T.A., Zeitler, P.K., and Hallet, B., 2011, Denudation of the Namche Barwa antiform, eastern Himalaya: Earth and Planetary Science Letters, v. 307, p. 323–333, doi:10.1016/j.epsl.2011.05.004.

Enlow, R.L., and Koons, P.O., 1998, Critical wedges in three dimensions: Analytical expressions from Mohr-Coulomb constrained perturbation analysis: Journal of Geophysical Research–Solid Earth, v. 103, no. B3, p. 4897–4914, doi:10.1029/97JB03209.

Finlayson, D.P., Montgomery, D.R., and Hallet, B., 2002, Spatial coincidence of rapid inferred erosion with young metamorphic massifs in the Himalayas: Geology, v. 30, p. 219–222, doi:10.1130/0091-7613(2002)030<0219:SCORIE>2.0.CO;2.

Finnegan, N.J., Hallet, B., Montgomery, D.R., Zeitler, P.K., Stone, J.O., Anders, A.M., and Liu, Y., 2008, Coupling of rock uplift and river incision in the Namche Barwa–Gyala Peri massif, Tibet, China: Geological Society of America Bulletin, v. 120, p. 142–155, doi:10.1130/B26224.1.

Gansser, A., 1964, Geology of the Himalayas: New York, Wiley-Interscience, 289 p.

Gansser, A., 1966, The Indian Ocean and the Himalayas: a geological interpretation: Eclogae Geologicae Helvetiae, v. 59, p. 831–848.

Garver, J.I., and Brandon, M.T., 1994, Erosional denudation of the British Columbia Coast Ranges as determined from fission-track ages of detrital zircon from the Tofino basin, Olympic Peninsula, Washington: Geological Society of America Bulletin, v. 106, p. 1398–1412, doi:10.1130/0016-7606(1994)106<1398:EDOTBC>2.3.CO;2.

Garver, J.I., Brandon, M.T., Roden-Tice, M., and Kamp, P.J.J., 1999, Exhumation history of orogenic highlands determined by detrital fission-track thermochronology, *in* Ring, U., Brandon, M.T., Lister, G.S., and Willett, S.D., eds., Exhumation Processes: Normal Faulting, Ductile Flow, and Erosion: Geological Society of London Special Publication 154, p. 283–304, doi:10.1144/GSL.SP.1999.154.01.13.

Gautam, P., and Fujiwara, Y., 2000, Magnetic polarity stratigraphy of Siwalik Group sediments of Karnali River section in western Nepal: Geophysical Journal International, v. 142, p. 812–824, doi:10.1046/j.1365-246x.2000.00185.x.

Geng, Q., Guitang, P., Zheng, L., Chen, Z., Fisher, R.D., Sun, Z., Chunsheng, O., Dong, H., Wang, X., Li, S., Lou, X., and Fu, H., 2006, The eastern Himalayan syntaxis: Major tectonic domains, ophiolitic mélanges and geologic evolution: Journal of Asian Earth Sciences, v. 27, p. 265–285, doi:10.1016/j.jseaes.2005.03.009.

Gilbert, G.K., 1914, Transportation of Debris by Running Water: U.S. Geological Survey Professional Paper 86, 263 p.

Gogoi, K.D., 1989, Stratigraphy and sedimentation of the Siwaliks of Arunachal Himalaya, northeast India, *in* Thanasuthipitak, T., and Ouchanum, P., eds., Proceedings of the International Symposium on Intermontane Basins: Geology and Resources: Chiang Mai, Thailand, Chiang Mai University, p. 427–451.

Goldthwait, R.P., 1971, Till: A Symposium: Wooster, Ohio, Ohio State University Press, 402 p.

Gradstein, F.M., Ogg, J.G., Schmitz, M., and Ogg, G., 2012, The Geologic Time Scale 2012: Amsterdam, Netherlands, Elsevier Publishing, p. 85–111.

Hallet, B., and Molnar, P., 2001, Distorted drainage basins as markers of crustal strain east of the Himalaya: Journal of Geophysical Research, v. 106, p. 13,697–13,709, doi:10.1029/2000JB900335.

Harrison, T.M., Yin, A., Grove, M., Lovera, O.M., Ryerson, F.J., and Zhou, X., 2000, The Zedong window: A record of superposed Tertiary convergence in southeastern Tibet: Journal of Geophysical Research, v. 105, no. B8, p. 19,211–19,230, doi:10.1029/2000JB900078.

Harrison, T.M., Célérier, J., Aikman, A., Hermann, J., and Heizler, M.T., 2009, Diffusion of ^{40}Ar in muscovite: Geochimica et Cosmochimica Acta, v. 73, p. 1039–1051, doi:10.1016/j.gca.2008.09.038.

Hasebe, N., Barbarand, J., Jarvis, K., Carter, A., and Hurford, A.J., 2004, Apatite fission-track chronometry using laser ablation ICP-MS: Chemical Geology, v. 207, p. 135–145, doi:10.1016/j.chemgeo.2004.01.007.

Heim, A., and Gansser, A., 1939, Central Himalaya: Geological Observations from the Swiss Expedition 1936: Zurich, Switzerland, Debruder Fretz, 246 p.

Holt, W.E., Ni, J.F., Wallace, T.C., and Haines, A.J., 1991, The active tectonics of the eastern Himalayan syntaxis and surrounding regions: Journal of Geophysical Research–Solid Earth, v. 96, p. 14,595–14,632, doi:10.1029/91JB01021.

Hoskin, P.W.O., and Schaltegger, U., 2003, The composition of zircon and igneous and metamorphic petrogenesis, *in* Hnachar, J.M., and Hoskin, P.W.O., eds., Zircon: Reviews of Mineralogy and Geochemistry, v. 53, p. 27–62.

Hoth, S., Adam, J., Kukowski, N., and Oncken, O., 2006, Influence of erosion on the kinematics of bivergent orogens: Results from scaled sandbox simulations, *in* Willet, S.D., Hovius, N., Brandon, M.T., and Fisher, D., eds., Tectonics, Climate and Landscape Evolution: Geological Society of America Special Paper 398, p. 201–225, doi:10.1130/2006.2398(12).

Hurford, A.J., and Green, P.F., 1983, The zeta age calibration of fission-track dating: Isotope Geoscience, v. 1, p. 285–317.

Jain, A.K., and Thakur, V.C., 1978, Abor volcanics of Arunachal Himalaya: Journal of the Geological Society of India, v. 19, no. 8, p. 335–349.

Jain, A.K., Thakur, V.C., and Tandon, S.K., 1974, Stratigraphy and structure of the Siang District, Arunachal (NEFA) Himalaya: Himalayan Geology, v. 4, p. 28–60.

Johnson, N.M., Stix, J., Tauxe, L., Cerveny, P.F., and Tahirkheli, R.A.K., 1985, Paleomagnetic chronology, fluvial processes and tectonic implications of the Siwalik deposits near Chinji village, Pakistan: The Journal of Geology, v. 93, p. 27–40, doi:10.1086/628917.

Karim, M.F., and Kennedy, J.F., 1990, Menu of coupled velocity and sediment-discharge relations for rivers: Journal of Hydraulic Engineering, v. 116, no. 8, p. 978–996, doi:10.1061/(ASCE)0733-9429(1990)116:8(978).

Karunakaran, C., and Ranga Rao, A., 1976, Status of Exploration for Hydrocarbons in the Himalayan Region—Contributions to Stratigraphy and Structure: Miscellaneous Publications of the Geological Survey of India 41, 66 p.

Kesari, G.K., 2010, Geology and Mineral Resources of Arunachal Pradesh: Miscellaneous Publications of the Geological Survey of India 30, 60 p.

Kirschvink, J.L., 1980, The least-squares line and plane and the analysis of paleomagnetic data: Geophysical Journal of the Royal Astronomical Society, v. 62, p. 699–718, doi:10.1111/j.1365-246X.1980.tb02601.x.

Koons, P.O., 1990, Two-sided orogen: Collision and erosion from the sandbox to the Southern Alps, New Zealand: Geology, v. 18, p. 679–682, doi:10.1130/0091-7613(1990)018<0679:TSOCAE>2.3.CO;2.

Koons, P.O., 1995, Modeling the topographic evolution of collisional belts: Annual Review of Earth and Planetary Sciences, v. 23, p. 375–408, doi:10.1146/annurev.ea.23.050195.002111.

Koons, P.O., Zeitler, P.K., Chamberlain, C.P., Craw, D., and Meltzer, A.S., 2002, Mechanical links between erosion and metamorphism in Nanga Parbat, Pakistan Himalaya: American Journal of Science, v. 302, p. 749–773, doi:10.2475/ajs.302.9.749.

Koons, P.O., Zeitler, P.K., and Hallet, B., 2013, Tectonic aneurysms and mountain building, *in* Owen, L.A., ed., Treatise on Geomorphology, Volume 5: Elsevier, 32 p., doi:10.1016/B978-0-12-374739-6.00094-4.

Korup, O., Montgomery, D.M., and Hewitt, K., 2010, Glacier and landslide feedbacks to topographic relief in the Himalayan syntaxes: Proceedings of the National Academy of Sciences of the United States of America, v. 107, no. 12, p. 5317–5322, doi:10.1073/pnas.0907531107.

Kumar, D., 1997, Geology of Arunachal Pradesh: Bangalore, Geological Society of India, 217 p.

Lallier, F., Antonie, C., Charreau, J., Caumon, G., and Ruiu, J., 2013, Management of ambiguities in magnetostratigraphic correlation: Earth and Planetary Science Letters, v. 371–372, p. 26–36, doi:10.1016/j.epsl.2013.04.019.

Lang, K.A., and Huntington, K.W., 2014, Antecedence of the Yarlung-Siang-Brahmaputra River, eastern Himalaya: Earth and Planetary Science Letters, v. 397, p. 145–158, doi:10.1016/j.epsl.2014.04.026.

Lang, K.A., Huntington, K.W., and Montgomery, D.R., 2013, Erosion of the Tsangpo Gorge by megafloods, eastern Himalaya: Geology, v. 41, p. 1003–1006, doi:10.1130/G34693.1.

Larsen, I.J., and Montgomery, D.R., 2012, Landslide erosion coupled to tectonics and river incision: Nature Geoscience, v. 5, p. 468–473, doi:10.1038/ngeo1479.

LeFort, P., 1975, Himalayas: The collided range. Present knowledge of the continental arc: American Journal of Science, v. 275A, p. 1–44.

Maclaren, J.M., 1904, The geology of Upper Assam: Records of the Geological Survey of India, v. 31, p. 179–209.

Malloy, M., 2004, Rapid Erosion at the Tsangpo Knickpoint and Exhumation of Southeastern Tibet [M.S. thesis]: Bethlehem, Pennsylvania, Lehigh University, 67 p.

Maluski, H., Proust, F., and Xiao, X.C., 1982, ^{39}Ar/^{40}Ar dating of the trans-Himalayan calc-alkaline magmatism of southern Tibet: Nature, v. 298, p. 152–154, doi:10.1038/298152a0.

Marques, F.O., and Cobbold, P.R., 2002, Topography as a major factor in the development of arcuate thrust belts: Insights from sandbox experiments: Tectonophysics, v. 348, p. 247–268, doi:10.1016/S0040-1951(02)00077-X.

Mathew, G., De Sarkar, S., Pande, K., Dutta, S., Ali, S., Rai, A., and Netrawali, S., 2013, Thermal metamorphism of the Arunachal Himalaya, India: Raman thermometry and thermochronological constraints on the tectono-thermal evolution: International Journal of Earth Sciences, v. 102, p. 1911–1936, doi:10.1007/s00531-013-0904-6.

Mathur, L.P., and Evans, P., 1964, Oil in India: New Delhi, 2nd International Geological Congress, 85 p.

McDougall, I., and Harrison, T.M., 1999, Geochronology and Thermochronology by the ^{40}Ar/^{39}Ar Method: New York, Oxford University Press, 269 p.

Miall, A.D., 1996, The Geology of Fluvial Deposits: Berlin, Springer, 582 p.

Middleton, G.V., and Southard, J.B., 1984, Mechanics of Sediment Movement: Lecture Notes for Short Course 3 (2nd ed.): Providence, Rhode Island, Society of Sedimentary Geology, 401 p., doi:10.2110/scn.84.03.

Misra, D.K., 2009, Litho-tectonic sequence and their regional correlation along the Lohit and Dibang valleys, eastern Arunachal Pradesh: Journal of the Geological Society of India, v. 73, p. 213–219, doi:10.1007/s12594-009-0077-x.

Misra, D.K., and Srivastava, P., 2009, River response to continuing movements along the active faults in the Siang valley, north-eastern Himalaya, India: Zeitschrift für Geomorphologie, v. 53, no. 4, p. 455–468, doi:10.1127/0372-8854/2009/0053-0455.

Montgomery, D.R., 2004, Observations on the role of lithology in strath terrace formation and bedrock channel width: American Journal of Science, v. 304, p. 454–476, doi:10.2475/ajs.304.5.454.

Montgomery, D.R., Hallet, B., Yuping, L., Finnegan, N., Anders, A., Gillespie, A., and Greenberg, H.M., 2004, Evidence for Holocene megafloods down the Tsangpo River gorge, southeastern Tibet: Quaternary Research, v. 62, no. 2, p. 201–207, doi:10.1016/j.yqres.2004.06.008.

Mugnier, J.L., Baby, P., Colletta, B., Vinour, P., Bale, P., and Leturmy, P., 1997, Thrust geometry controlled by erosion and sedimentation: A view from analogue models: Geology, v. 25, p. 427–430, doi:10.1130/0091-7613(1997)025<0427:TGCBEA>2.3.CO;2.

Najman, Y., 2006, The detrital record of orogenesis: A review of approaches and techniques used in the Himalayan sedimentary basins: Earth-Science Reviews, v. 74, p. 1–72.

Najman, Y., Garzanti, E., Pringle, M., Bickle, M., Stix, J., and Khan, I., 2003, Early-middle Miocene paleodrainage and tectonics in the Pakistan Himalaya: Geological Society of America Bulletin, v. 115, no. 10, p. 1265–1277, doi:10.1130/B25165.1.

Najman, Y., Bickle, M., Garzanti, E., Pringle, M., Barford, D., Brozovic, N., Burbank, D., and Ando, S., 2009, Reconstructing the exhumation history of the Lesser Himalaya, NW India, from a multitechnique provenance study of the foreland basin Siwalik Group: Tectonics, v. 28, no. 5, p. 1–15, doi:10.1029/2009TC002506.

Novak, B., Housen, B., Kitamura, Y., Kanamatsu, K., and Kawamura, K., 2014, Magnetic fabric analyses as a method for determining sediment transport and

deposition in deep sea sediments: Marine Geology, v. 356, p. 19–30, doi:10.1016/j.margeo.2013.12.001.

Ojha, T.P., Butler, R.F., Quade, J., DeCelles, P.G., Richards, D., and Upreti, B.N., 2000, Magnetic polarity stratigraphy of the Neogene Siwalik Group at Khutia Khola, far western Nepal: Geological Society of America Bulletin, v. 112, p. 424–434, doi:10.1130/0016-7606(2000)112<424:MPSOTN>2.0.CO;2.

Ojha, T.P., Butler, R.F., DeCelles, P.G., and Quade, J., 2009, Magnetic polarity stratigraphy of the Neogene foreland basin deposits of Nepal: Basin Research, v. 21, p. 61–90, doi:10.1111/j.1365-2117.2008.00374.x.

Pan, G., Ding, J., Yao, D., and Wang, L., 2004, Geological Map of Qinhai-Xizhang (Tibet) and Adjacent Areas: Chengdu, Chengdu Cartographic Publishing House, scale 1:1,500,000, 6 sheets.

Peltzer, G., and Tapponnier, P., 1988, Formation and evolution of strike-slip faults, rifts, and basins during the India-Asia collision: An experimental approach: Journal of Geophysical Research, v. 93, no. B12, p. 15,085–15,117, doi:10.1029/JB093iB12p15085.

Pik, R., France-Lanord, C., and Carignan, J., 2005, Extreme uplift and erosion rates in eastern Himalayas (Siang-Brahmaputra basin) revealed by detrital (U-Th)/He thermochronology: Geophysical Research Abstracts, v. 7, 2 p, SRef-ID: 1607-7962/gra/EGU05-A-09421.

Pilgrim, G.E., 1913, The correlation of the Siwaliks with the mammal horizons of Europe: Records of the Geological Survey of India, v. 43, p. 264–325.

Ranga Rao, A., 1983, Geology and hydrocarbon potential of a part of Assam-Arakan basin and its adjacent region, *in* Bhandari, L.L., Venkatachala, B.S., Kumar, R., Swamy, S.N., Garga, P., and Srivastava, D.C., eds., Petroliferous Basins of India: Petroleum Asia Journal, v. 6, p. 112–127.

Ring, W., Brandon, M.T., Willet, S.D., and Lister, G.S., 1999, Exhumation processes, *in* Ring, U., Brandon, M.T., Lister, G.S., and Willett, S.D., eds., Exhumation Processes: Normal Faulting, Ductile Flow, and Erosion: Geological Society of London Special Publication 154, p. 1–27, doi:10.1144/GSL.SP.1999.154.01.01.

Robert, X., van der Beek, P., Braun, J., Perry, C., and Mugnier, J.-L., 2011, Control of detachment geometry on lateral variations in exhumation rates in the Himalaya: Insights from low-temperature thermochronology and numerical modeling: Journal of Geophysical Research, v. 116, p. B05202, doi:10.1029/2010JB007893.

Ruhl, K.W., and Hodges, K.V., 2005, The use of detrital mineral cooling ages to evaluate steady state assumptions in active orogens: An example from the central Nepalese Himalaya: Tectonics, v. 24, p. TC4015, doi:10.1029/2004TC001712.

Ruiz, G., and Seward, D., 2006, The Punjab foreland basin of Pakistan: A reinterpretation of zircon fission-track data in the light of Miocene hinterland dynamics: Terra Nova, v. 18, no. 4, p. 248–256, doi:10.1111/j.1365-3121.2006.00686.x.

Schneider, D.A., Edwards, M.A., Kidd, W.S.F., Asif Khan, M., Seeber, L., and Zeitler, P.K., 1999a, Tectonics of Nanga Parbat, western Himalaya: Synkinematic plutonism within the double vergent shear zones of a crustal scale pop-up structure: Geology, v. 27, no. 11, p. 999–1002, doi:10.1130/0091-7613(1999)027<0999:TONPWH>2.3.CO;2.

Schneider, D.A., Edwards, M.A., Kidd, W.S.F., Zeitler, P.K., and Coath, C.D., 1999b, Early Miocene anatexis identified in the western syntaxis, Pakistan Himalaya: Earth and Planetary Science Letters, v. 167, no. 3–4, p. 121–129, doi:10.1016/S0012-821X(99)00022-9.

Schwarz, W.H., and Trieloff, M., 2007, Intercalibration of ^{40}Ar-^{39}Ar age standards NL-25, HB3gr hornblende, GA1550, SB-3, HD-B1 biotite and BMus/2 muscovite: Chemical Geology, v. 242, p. 218–231, doi:10.1016/j.chemgeo.2007.03.016.

Searle, M.P., Windley, B.F., Coward, M.P., Cooper, D.J.W., Rex, A.J., Rex, D., Tingdong, L., Xuchang, X., Jan, M.Q., Thakur, V.C., and Kumar, S., 1987, The closing of Tethys and the tectonics of the Himalaya: Geological Society of America Bulletin, v. 98, no. 6, p. 678–701, doi:10.1130/0016-7606(1987)98<678:TCOTAT>2.0.CO;2.

Seward, D., and Burg, J.-P., 2008, Growth of the Namche Barwa syntaxis and associated evolution of the Tsangpo Gorge: Constraints from structural and thermochronological data: Tectonophysics, v. 451, p. 282–289, doi:10.1016/j.tecto.2007.11.057.

Simpson, G., 2004, Role of river incision in enhancing deformation: Geology, v. 32, p. 341–344, doi:10.1130/G20190.2.

Simpson, G., 2006, Influence of erosion and deposition on deformation in fold belts, *in* Willet, S.D., Hovius, N., Brandon, M.T., and Fisher, D., eds., Tectonics, Climate and Landscape Evolution: Geological Society of America Special Paper 398, p. 267–281, doi:10.1130/2006.2398(16).

Singh, G., 1975, First report of vertebrate fossil from Arunachal Pradesh: Geological Survey of India News, v. 6, no. 2, p. 279–297.

Singh, G., 1976, On the stratigraphic correlation of Upper Tertiary of Arunachal Pradesh: Geological Survey of India Miscellaneous Publication 43, p. 82–84.

Singh, S., 1993, Geology and tectonics of the eastern syntaxial bend: Arunachal Himalaya: Journal of Himalayan Geology, v. 4, no. 2, p. 149–163.

Singh, T., 1999, Paleontological records from the eastern Himalaya: A synthesis, *in* Verma, P.K., ed., Geological Studies in the Eastern Himalayas: Delhi, Pilgrim Books, p. 129–163.

Singh, T., and Prakash, U., 1980, Leaf impressions from the Siwalik sediments of Arunachal Pradesh, India: Geophytology, v. 10, p. 104–107.

Singh, T., and Tripathi, S.K.M., 1989, Siwalik sediments of Arunachal Himalaya: Palynology, Palaeoecology and Palaeogeography, v. 38, p. 325–332.

Singh, T., Srivastava, R.A.K., and Kumar, S., 1982, Sedimentology of the Siwalik sandstones of Subansiri district, Arunachal Pradesh: Himalayan Geology, v. 9, p. 422–430.

Sol, S., Meltzer, A., Burgmann, R., van der Hilst, R.D., King, R., Chen, Z., Koons, P.O., Lev, E., Liu, Y.P., Zeitler, P.K., Zhang, X., Zhang, J., and Zurek, B., 2007, Geodynamics of the southeastern Tibetan Plateau from seismic anisotropy and geodesy: Geology, v. 35, p. 563–566, doi:10.1130/G23408A.1.

Steiger, R.J., and Jäger, E., 1977, Subcommission on Geochronology: Convention on the use of decay constants in geo- and cosmochronology: Earth and Planetary Science Letters, v. 36, p. 359–362, doi:10.1016/0012-821X(77)90060-7.

Stewart, R.J., Hallet, B., Zeitler, P.K., Malloy, M.A., Allen, C.M., and Trippett, D., 2008, Brahmaputra sediment flux dominated by highly localized rapid erosion from the easternmost Himalaya: Geology, v. 36, p. 711–714, doi:10.1130/G24890A.1.

Szulc, A., Najman, Y., Sinclair, H., Pringle, M., Bickle, M., Chapman, H., Garzanti, E., Ando, S., Huyghe, P., Mugnier, J.-L., Ojha, T., and DeCelles, P., 2006, Tectonic evolution of the Himalaya constrained by detrital ^{40}Ar-^{39}Ar, Sm-Nd and petrographic data from the Siwalik foreland basin succession, SW Nepal: Basin Research, v. 18, p. 375–391, doi:10.1111/j.1365-2117.2006.00307.x.

Taira, A., 1989, Magnetic fabrics and depositional processes, *in* Taira, A., and Masuda, F., eds., Sedimentary Facies in the Active Plate Margin: Tokyo, Japan, Terra Scientific Publishing, p. 43–77.

Tapponnier, P., Lacassin, R., Leloup, P.H., Schärer, U., Dalai, Z., Haiwei, W., Xiaohan, L., Shaocheng, J., Lianshang, Z., and Jiayou, Z., 1990, The Ailao Shan/Red River metamorphic belt: Tertiary left-lateral shear between Indochina and South China: Nature, v. 343, p. 431–437, doi:10.1038/343431a0.

Tauxe, L., 1998, Paleomagnetic Principles and Practice: Dordrecht, The Netherlands, Kluwer Academic Publishers, 299 p.

Tauxe, L., Kylstra, N., and Constable, C., 1991, Bootstrap statistics for paleomagnetic data: Journal of Geophysical Research, v. 96, p. 11,723–11,740, doi:10.1029/91JB00572.

Treloar, P.J., and Coward, M.O., 1991, Indian plate motion and shape: Constraints on the geometry of the Himalayan orogeny: Tectonophysics, v. 191, p. 189–198, doi:10.1016/0040-1951(91)90055-W.

Uddin, A., Hames, W.E., and Zahid, K.M., 2010, Laser ^{40}Ar/^{39}Ar constraints on Miocene sequences from the Bengal basin: Implications for middle Miocene denudation of the eastern Himalayas: Journal of Geophysical Research–Solid Earth, v. 115, p. B7, p. B07416, doi:10.1029/2009JB006401.

van Rijn, L.C., 1984, Sediment transport: Part 1. Bed load transport: Journal of Hydraulic Engineering, v. 110, no. 10, p. 1431–1456, doi:10.1061/(ASCE)0733-9429(1984)110:10(1431).

Verma, R.K., and Mukhopadhyay, M., 1977, An analysis of the gravity field in northeastern India: Tectonophysics, v. 42, p. 283–317, doi:10.1016/0040-1951(77)90171-8.

Vermeesch, P., 2004, How many grains are needed for a provenance study?: Earth and Planetary Science Letters, v. 224, no. 3–4, p. 441–451, doi:10.1016/j.epsl.2004.05.037.

Vermeesch, P., 2012, On the visualization of detrital age distributions: Chemical Geology, v. 312–313, p. 190–194, doi:10.1016/j.chemgeo.2012.04.021.

Wadia, D.N., 1931, The syntaxis of the northwest Himalaya: Its rocks, tectonics and orogeny: Records of the Geological Survey of India, v. 65, p. 189–220.

Walker, R.G., and Cant, D.J., 1984, Sandy fluvial systems, *in* Walker, R.G., ed., Facies Models (2nd ed.): Geoscience Canada Reprint Series 1, p. 71–89.

Wang, P., Scherler, D., Liu-Zeng, J., Mey, J., Avouac, J.-P., Zhang, Y., and Shi, D., 2014, Tectonic control of Yarlung Tsangpo Gorge revealed by a buried canyon in southern Tibet: Science, v. 346, no. 6212, p. 978–981, doi:10.1126/science.1259041.

Warren, C., Singh, A.K., Riberts, N.M.W., Regis, D., Halton, A.M., and Singh, R.B., 2014, Timing and conditions of peak metamorphism and cooling across the Zimithang thrust, Arunachal Pradesh, India: Lithosphere, v. 200–201, p. 94–110.

Whipp, D.M., Ehlers, T.A., Braun, J., and Spath, C.D., 2009, Effects of exhumation kinematics and topographic evolution on detrital thermochronometer data: Journal of Geophysical Research–Earth Surface, v. 114, p. F04021, doi:10.1029/2008JF001195.

Whipple, K.X., and Meade, B.J., 2004, Controls on the strength of coupling among climate, erosion and deformation in two-sided, frictional orogenic wedges at steady state: Journal Geophysical Research–Earth Surface, v. 109, p. F1, doi:10.1029/2003JF000019.

Whipple, K.X., and Tucker, G.E., 1999, Dynamics of the stream-power river incision model: Implications for height limits of mountain ranges, landscape response timescales, and research needs: Journal of Geophysical Research, v. 104, p. 17,661–17,674, doi:10.1029/1999JB900120.

White, N., Pringle, M., Garzanti, E., Bickle, M., Najman, Y., Chapman, H., and Friend, P., 2002, Constraints on the exhumation and erosion of the High Himalayan slab, NW India, from foreland basin deposits: Earth and Planetary Science Letters, v. 195, no. 1–2, p. 29–44, doi:10.1016/S0012-821X(01)00565-9.

Willet, S., 1999, Orogeny and orography: The effects of erosion on the structure of mountain belts: Journal of Geophysical Research–Solid Earth, v. 104, no. B12, doi:10.1029/1999JB900248.

Willett, S., and Brandon, M.T., 2002, On steady states in mountain belts: Geology, v. 30, p. 175–178, doi:10.1130/0091-7613(2002)030<0175:OSSIMB>2.0.CO;2.

Winslow, D.M., Zeitler, P.K., Chamberlain, C.P., and Hollister, L.S., 1994, Direct evidence for a steep geotherm under conditions of rapid denudation, Western Himalaya, Pakistan: Geology, v. 22, no. 12, p. 1075–1078, doi:10.1130/0091-7613(1994)022<1075:DEFASG>2.3.CO;2.

Winslow, D.M., Zeitler, P.K., Chamberlain, C.P., and Williams, I.S., 1996, Geochronologic constraints on syntaxial development in the Nanga Parbat region, Pakistan: Tectonics, v. 15, p. 1292–1308, doi:10.1029/96TC00032.

Yalin, M.S., 1972, Mechanics of Sediment Transport: New York, Pergamon Press, 290 p.

Yin, A., 2006, Cenozoic tectonic evolution of the Himalayan orogen as constrained by along-strike variation of structural geometry, exhumation history, and foreland sedimentation: Earth-Science Reviews, v. 76, no. 1–2, p. 1–131, doi:10.1016/j.earscirev.2005.05.004.

Yin, A., and Harrison, T.M., 2000, Geologic evolution of the Himalayan-Tibetan orogen: Annual Review of Earth and Planetary Sciences, v. 28, p. 211–280, doi:10.1146/annurev.earth.28.1.211.

Yin, A., Dubey, C.S., Kelty, T.K., Webb, A.A.G., Harrison, T.M., Chou, C.Y., and Celerier, J., 2010, Geologic correlation of the Himalayan orogeny and Indian craton: Part 2. Structural geology, geochronology and tectonic evolution of the eastern Himalaya: Geological Society of America Bulletin, v. 122, p. 360–395, doi:10.1130/B26461.1.

Zeitler, P.K., Johnson, N.M., Naeser, C.W., and Tahirkheli, R.A.K., 1982, Fission-track evidence for Quaternary uplift of the Nanga Parbat region, Pakistan: Nature, v. 298, p. 255–257, doi:10.1038/298255a0.

Zeitler, P.K., Chamberlain, C.P., and Smith, H.A., 1993, Synchronous anatexis, metamorphism and rapid denudation at Nanga Parbat, Pakistan Himalaya: Geology, v. 21, p. 347–350, doi:10.1130/0091-7613(1993)021<0347:SAMARD>2.3.CO;2.

Zeitler, P.K., Meltzer, A.S., Koons, P.O., Craw, D., Hallet, B., Chamberlain, C.P., Kidd, W.S.F., Park, S.K., Seeber, L., Bishop, M., and Shroder, J., 2001, Erosion, Himalayan geodynamics, and the geomorphology of metamorphism: GSA Today, v. 11, no. 1, p. 4–9, doi:10.1130/1052-5173(2001)011<0004:EHGATG>2.0.CO;2.

Zeitler, P.K., Meltzer, A.S., Brown, L., Kidd, W.S.F., Lim, C., and Enkelmann, E., 2014, Tectonics and topographic evolution of Namche Barwa and the easternmost Lhasa block, Tibet, *in* Nie, J., Horton, B.K., and Hoke, G.D., eds., Toward an Improved Understanding of Uplift Mechanisms and the Elevation History of the Tibetan Plateau: Geological Society of America Special Paper 507, 23 p., doi:10.1130/2014.2507(02).

Zeitler, P.K., Koons, P.O., Hallet, B., and Meltzer, A.S., 2015, Comment on "Tectonic control of Yarlung Tsangpo Gorge revealed by a buried canyon in southern Tibet": Science, v. 349, no. 6250, p. 799, doi:10.1126/science.aaa9380.

Zhang, J.Y., Yin, A., Liu, W.C., Wu, F.Y., Lin, D., and Grove, M., 2012, Coupled U-Pb dating and Hf isotopic analysis of detrital zircon of modern river sand from the Yalu River (Yarlung Tsangpo) drainage system in southern Tibet: Constraints on the transport processes and evolution of Himalayan rivers: Geological Society of America Bulletin, v. 124, p. 1449–1473, doi:10.1130/B30592.1.

Science Editor: Aaron Cavosie
Associate Editor: An Yin

Manuscript Received 2 September 2015
Revised Manuscript Received 29 January 2016
Manuscript Accepted 31 March 2016

Printed in the USA